Regional variations in bulk chemistry, mineralogy, and the compositions of mafic and accessory minerals in the batholiths of California

JAY J. AGUE*
GEORGE H. BRIMHALL } *Department of Geology and Geophysics, University of California, Berkeley, California 94720*

ABSTRACT

We define regional variations in mafic and accessory mineral assemblages and compositions and expand the current understanding of spatial variations in whole-rock geochemistry in the batholiths of California. In so doing, we gain new insights into the nature of magmatic source rocks and mechanisms of magma generation in volcano-plutonic arcs of active continental margins. Little-studied metaluminous to strongly peraluminous granites containing Fe-rich biotite with $\log(X_{Mg}/X_{Fe}) < -0.21$ (I-SCR type; strongly contaminated and reduced I-type) typically occur in north-northwest–striking belts within pre-batholithic wall-rock terranes containing graphitic pelites in the western Sierra Nevada and Peninsular Ranges batholiths. The other pluton types (I-WC, I-MC, and I-SC; weakly, moderately, and strongly contaminated, but not reduced, I-types) range in composition from metaluminous to weakly peraluminous and form a general west-to-east progression across the batholiths defined by increasing F/OH in biotite. This correlates with the well-known petrologic sequence from quartz diorites and granodiorites on the west to quartz monzonites and granites to the east. I-WC types also occur in the central-eastern Sierra Nevada batholith, however, primarily in the vicinity of the Independence dike swarm.

F/OH and Mn in biotite and amphibole increase on a regional scale from western I-WC types to eastern I-MC and I-SC types, parallel to eastward increases in incompatible elements and decreases in compatible elements in the plutons. In contrast, the belts of western I-SCR granites and eastern I-WC quartz diorites and granodiorites disrupt the regional west-to-east systematics in both mineral and whole-rock geochemistry. Spatial variations in the Al content of amphibole are regional in scale and reflect pressures of pluton crystallization. We conclude that significant, previously unrecognized complexity exists in regional geochemical systematics in the California batholiths.

INTRODUCTION

The granitic batholiths of California have long been the focus of varied petrologic and isotopic research directed at interpreting geological factors which control the chemistry of melts generated and emplaced at plate margins where oceanic and continental crust interact by subduction. Pronounced transverse asymmetries with north-northwest longitudinal continuity have been recognized in the petrologic, geochemical, isotopic, and geochronologic character of the batholiths. Herein, in order to clarify spatial variations in magmatic source-region characteristics as well as mechanisms of magma–wall-rock interaction causing regional plutonic compositional trends, we present new data on common rock-forming and accessory mineral chemistry. Our approach, briefly outlined in Ague and Brimhall (1987) and developed here in greater detail, contributes to the further development and refinement of the regional geologic context of the California batholiths, particularly the controls on magma chemistry imposed by the localized occurrence of highly reducing, pre-batholithic wall-rock terranes and regional-scale variations in the thickness and metamorphic grade of cratonal basement. We focus on the spatial variation in complex solid-solution compositions and assemblages which reflect a number of factors in magmatic evolution such as redox effects and magmatic halogen content which have previously not received sufficient attention.

Lindgren (1915) was the first to document the fact that in general, the batholiths of western North America become increasingly felsic from west to east. Transverse variations in whole-rock chemistry exist in the central Sierra Nevada batholith which correlate with the west-to-east petrologic variations described by Lindgren (1915) (compare with Moore, 1959; Dickinson, 1970; Bateman and Dodge, 1970; Dodge, 1972). Stable- and radiogenic-isotope studies in both the Sierra Nevada and Peninsular Ranges batholiths (compare with Kistler and Peterman, 1973; Early and Silver, 1973; Taylor and Silver, 1978; DePaolo, 1981; Masi and others, 1981; Nelson and DePaolo, 1985) have broadly identified likely magmatic source components and processes of mixing and delineated the probable edge of the Precambrian craton of western North America. A geochronologic framework for these batholiths has been established (see Evernden and Kistler, 1970; Silver and others, 1979; Saleeby, 1981; Stern and others, 1981; Chen and Moore, 1982), detailing the intrusion of plutons in space and time. Systematic regional variations in the age and lithologic character of pre-batholithic wall-rock terranes (Nokleberg, 1983), as well as regional metallogenic patterns, have been documented (Albers, 1981).

Because a comprehensive petrologic framework exists for the California batholiths, this magmatic arc provides an ideal field region to apply new methods directed at further elucidating batholith formation processes at convergent plate boundaries. Our methods (Ague and Brimhall, 1987), involve the systematic study of

*Present address: Department of Geology and Geophysics, Yale University, P.O. Box 6666, New Haven, Connecticut 06511.

Additional material for this article (appendices) may be obtained free of charge by requesting Supplementary Data 8813 from the GSA Documents Secretary.

Geological Society of America Bulletin, v. 100, p. 891–911, 20 figs., 2 tables, June 1988.

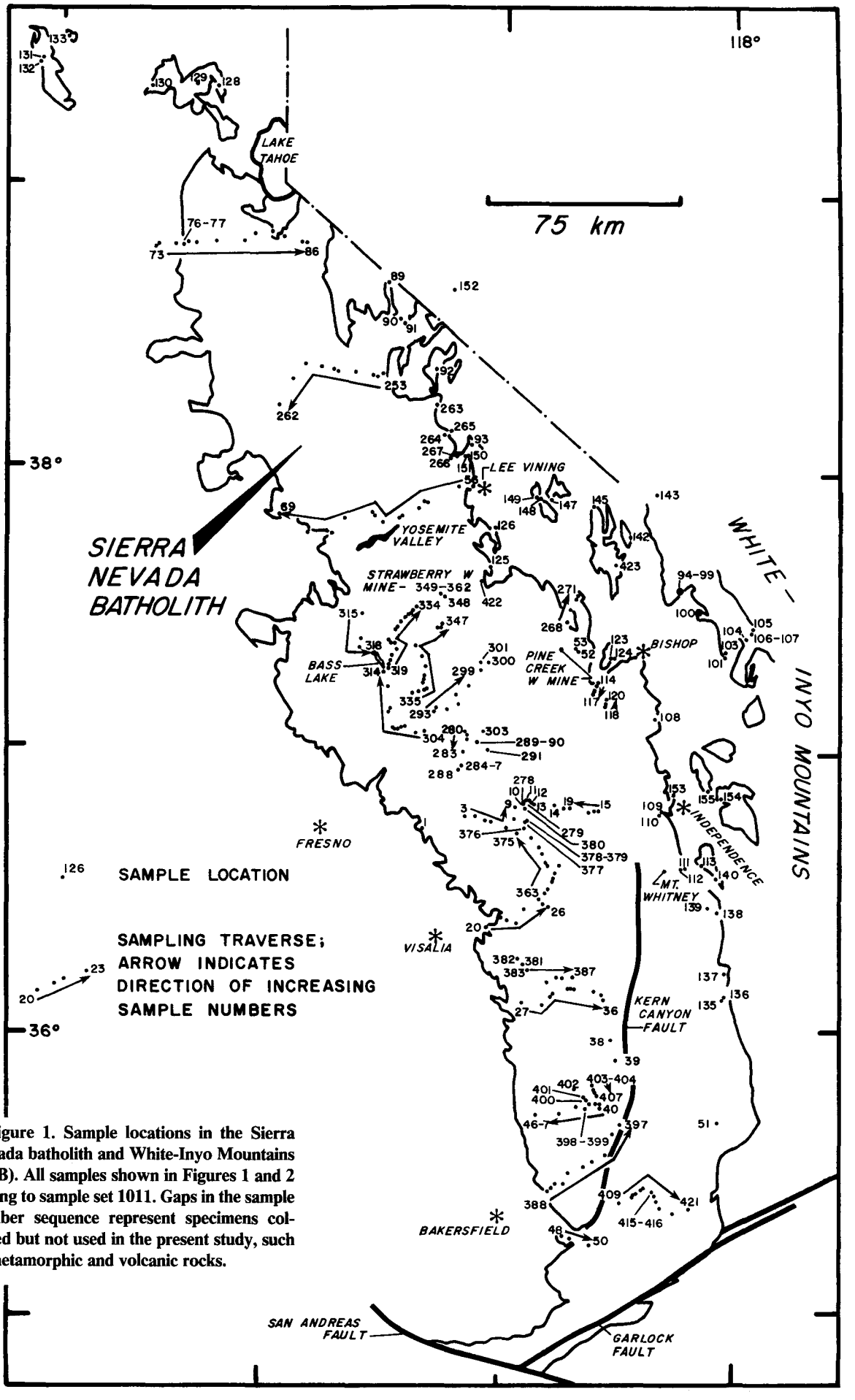

Figure 1. Sample locations in the Sierra Nevada batholith and White-Inyo Mountains (SNB). All samples shown in Figures 1 and 2 belong to sample set 1011. Gaps in the sample number sequence represent specimens collected but not used in the present study, such as metamorphic and volcanic rocks.

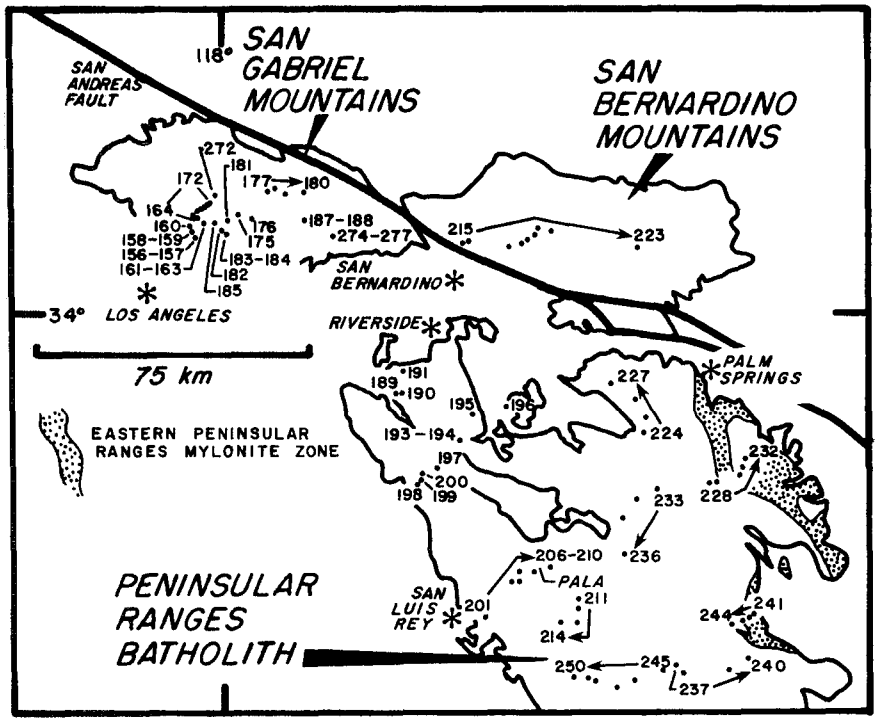

Figure 2. Sample locations in the northern Peninsular Ranges batholith (PRB), San Bernardino Mountains (SBB), and the San Gabriel Mountains (SGB). Position of eastern Peninsular Ranges mylonite zone from Erskine (1985).

key mafic and accessory mineral compositions and assemblages, coupled with whole-rock geochemistry and regional distributions of geochemically distinct intrusive types, to refine interpretations of source materials involved in batholith generation and to provide new insight into the depth of exposure of the plutons. Our conclusions therefore bear directly upon such important problems as the generation of "S-type" granites in the western United States (Chappell and White, 1974; White and others, 1986), the petrologic regimes required to produce magnetite- and ilmenite-series plutons (Czamanske and others, 1981), the geochemical effects of contamination of mafic magmas with different types of crustal materials, and the magmatic processes operative in the crust as a function of depth.

In order to define regional geochemical trends accurately and in sufficient detail, we have carried out a regional-scale sampling program. We utilize a total of 393 samples of granitic rocks collected along numerous sampling traverses across the Sierra Nevada batholith and White-Inyo Mountains (SNB), the northern Peninsular Ranges batholith (PRB), the San Bernardino fault block (SBB), and the San Gabriel fault block (SGB) (Figs. 1, 2). The analysis of a large number of systematically collected samples has allowed us to generate a comprehensive geochemical data base with a high degree of internal consistency. A complete set of geochemical and mineralogical data for all samples and localities studied is available.[1]

Ague and Brimhall (1987) presented a classification scheme for granitic rocks of the batholiths using the composition of plutonic biotite as determined by electron microprobe. The rationale for choosing biotite is simple. Biotite is widely distributed in granitic magmatic and hydrothermal systems and has a complex crystal chemistry, with the metals Mg, Fe, Mn, Ti, and Al octahedrally coordinated to OH, F, and Cl. Biotite compositions, under the provision that other minerals enter into an array of useful equilibrium buffering relationships, thus relate directly to important magmatic and hydrothermal variables such as oxygen fugacity, water fugacity, f_{HF}/f_{H_2O}, and f_{HF}/f_{HCl} (Wones and Eugster, 1965; Brimhall and others, 1983, 1985; Munoz, 1984). Here, we have extended our study to plutonic amphiboles which provide critical data regarding the depths of emplacement of the plutons (Hammarstrom and Zen, 1986).

We utilize a $\log(X_F/X_{OH})$ versus $\log(X_{Mg}/X_{Fe})$ coordinate framework for biotite classification (Fig. 3A) because as part of ubiquitous buffer assemblages, these variables reflect the f_{O_2} and f_{HF}/f_{H_2O} conditions of biotite crystallization. In addition, in the biotite structure, F and OH are the primary substitutional anions in the hydroxyl site, whereas Mg and Fe are the predominant elements in octahedral sites. Rocks containing biotite with $\log(X_{Mg}/X_{Fe}) > -0.21$ are divided into three subgroups based upon increasing F/OH: (1) I-WC type (weakly contaminated I-type), (2) I-MC type (moderately contaminated I-type), and (3) I-SC type (strongly contaminated I-type). Reduced rocks containing biotite with $\log(X_{Mg}/X_{Fe}) < -0.21$ are classified as I-SCR type (strongly contaminated and reduced I-type). The term "contamination" is used here in a broad sense to refer to interactions of mafic "I-type" magmas derived from the upper mantle, deep crust, or subducted slabs with continental crustal source components, which may have spatially variable characteristics (compare with Farmer and DePaolo, 1983), by such processes as partial melting, magma mixing, and assimilation. We note in this context that mantle-derived rocks of "M-type," discussed first by White (1979) in abstract form, are here broadly classified as "I-type" for simplicity.

Figure 3B illustrates the spatial distributions of the rock types. The well-known petrologic sequence from western quartz diorites and granodiorites to eastern quartz monzonites and granites is broadly paralleled by the west-to-east progression from I-WC to I-SC types (Ague and Brimhall, 1987). Figure 3B, however, demonstrates that significant additional complexity exists in the regional distributions of I-SCR granites and I-WC types. The I-SCR granites occur primarily in narrow north-northwest–striking belts within pre-batholithic wall-rock terranes containing graphitic pelites in the western SNB and PRB, regions thought previously to be characterized by much more mafic intrusives (Ague and Brimhall, 1987). On the other hand, I-WC–type mafic quartz diorites and granodiorites are present in the eastern SNB in the vicinity of the Independence dike swarm (Chen and Moore, 1979) (immediately north of B′) and seem out of place there, given the regional petrologic systematics documented by Moore (1959). Although the eastward I-WC to I-MC and I-SC progression almost certainly requires the involvement of cratonal magmatic source components in the generation of the eastern batholiths (compare with Kistler and Peterman, 1973; Silver and others, 1979; DePaolo, 1981; Ague and Brimhall, 1987), the previously little-studied western I-SCR and eastern I-WC belts reflect the operation of distinct magmatic processes associated with intrusion of calc-alkaline magmas into reducing pelitic wall-rock terranes in the former case and regions of thin or perhaps absent continental crust in the latter.

[1]Appendices A–F may be obtained free of charge by requesting Supplementary Data 8813 from the GSA Documents Secretary.

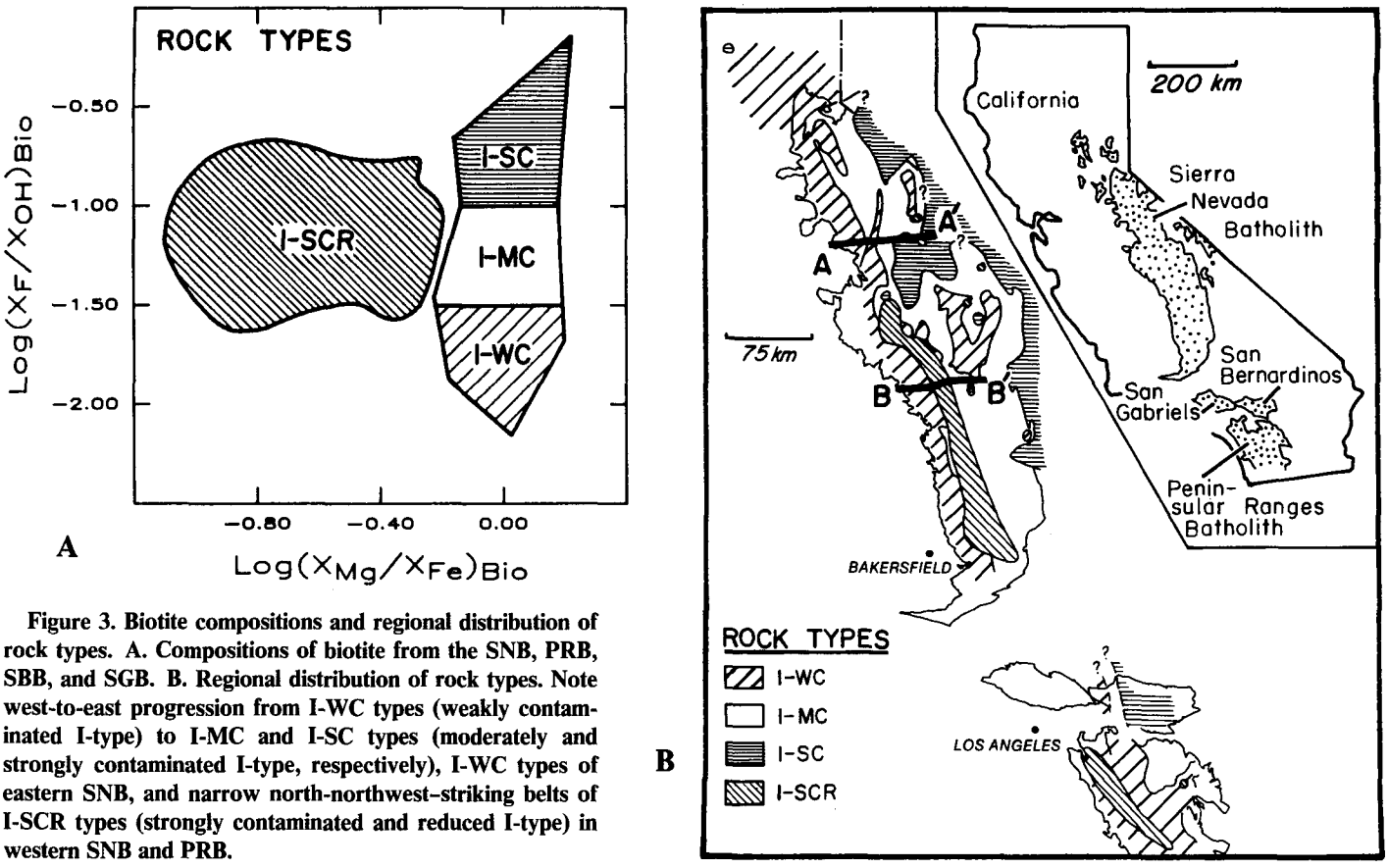

Figure 3. Biotite compositions and regional distribution of rock types. A. Compositions of biotite from the SNB, PRB, SBB, and SGB. B. Regional distribution of rock types. Note west-to-east progression from I-WC types (weakly contaminated I-type) to I-MC and I-SC types (moderately and strongly contaminated I-type, respectively), I-WC types of eastern SNB, and narrow north-northwest-striking belts of I-SCR types (strongly contaminated and reduced I-type) in western SNB and PRB.

In this paper, we first discuss regional whole-rock geochemical systematics and the petrologic character of these intrusive types and examine in detail the geochemistry of the mafic silicates and key accessory minerals which they contain. We then discuss the regional distribution of mineral assemblages and gradients, trends, and discontinuities in mafic mineral composition in the California batholiths. In the second part of this paper (Ague and Brimhall, 1988, this volume), we interpret petrologic controls on regional asymmetries in the geochemical character of the batholiths and the anomalous belts of I-SCR and I-WC intrusives. Our conclusions are based on calculated magmatic f_{HF}/f_{H_2O}, $T-f_{O_2}$ relations, crystallization pressure, probable magmatic source-component geochemistry, published isotopic and age data, and critical geologic field relations. In the third part of this work (Brimhall and Ague, 1988), we investigate the global compositional systematics of igneous and hydrothermal biotites from base-metal ore deposits in an effort to understand the nature of magmatic source rocks giving rise to base-metal mineralization and to gain further insights into processes of hydrothermal alteration and ore deposition occurring during the transition from magmatic to magmatic-hydrothermal conditions.

ANALYTICAL TECHNIQUES

Electron Microprobe Analysis

Because a large number of samples are needed to define accurately regional patterns in mineral composition, mineral phases must be analyzed rapidly and under essentially identical conditions to insure the internal consistency of the data base. In order to maximize internal consistency, we have (1) provided for the relocation of probed points by computer, which insures accurate repositioning for multiple analyses, and (2) analyzed a large number of samples during individual probe runs.

Mineral analyses were carried out using a semi-automated 8-channel ARL SEMQ electron microprobe operated with an accelerating voltage of 15 kV and a sample current of 25 nA (on brass). Because 2 probe runs are needed to perform a 12-element analysis on the ARL instrument, the same point on a mineral grain must be located twice for chemical analysis and zoning profiles. To facilitate relocation, the digitizing petrographic microscope (DPM) of Brimhall (1979) and Brimhall and Rivers (1985) was used. Modal analyses were also performed utilizing the DPM. In order to minimize the effects of instrument drift and carbon coat irregularities, phases from as many as 32 samples were analyzed in a single probe run using 4 composite epoxy probe mounts, each containing as many as 8 ¼-in.-diameter rock cores.

Major and minor oxides were analyzed using natural biotite, kaersutite, hornblende, orthoclase, and ilmenite as standards. Natural sodalite (6.84 wt. % Cl) was used as a Cl standard, and synthetic fluor-phlogopite (9.02 wt.% F) and a natural biotite (4.02 wt.% F) were utilized for F. PET (pentaerythritol) and TAP (thallium acid phthalate) crystals were utilized for Cl and F analysis, respectively. On the basis of analyses of a number of F-bearing standards, we estimate the accuracy of the F analysis for a given mineral to be within 10% of the actual value. Microprobe data were reduced with standard Bence-Albee-type correction factors (Bence and Albee, 1968; Albee and Ray, 1970). The number of analysis points per grain varies from 5 to 13 for the mafic silicates and from 3 to 14 for the accessory phases.

Whole-Rock XRF Analyses

Whole-rock major, minor, and trace elements were determined by energy-dispersive X-ray fluorescence (XRF) techniques (J. Hampel, analyst). Major- and minor-element analyses were performed on glass plates of fused rock samples, whereas trace elements were determined on pressed pills using a cellulose binder. Major and minor elements were determined using U.S. Geological Survey standards BCR-1 and W-1 and the following standards analyzed wet chemically by I.S.E. Carmichael: LHG, 780-K18, 867-311, and 913-8016. One additional standard, Napa glass, analyzed by M. S. Ghiorso, was also utilized. Trace elements were determined using U.S. Geological Survey standards G-2 and W-1. Precisions for all major and minor oxides except K_2O and Na_2O were better than 1%, whereas K_2O, Na_2O, and trace-element precisions were better than 5%.

WHOLE-ROCK CHEMISTRY

We have analyzed 44 samples of the SNB sample set for major and minor elements and 114 samples for trace elements in order to elucidate spatial variations in pluton geochemistry and to investigate relationships between mafic silicate chemistry, mineral assemblage, and whole-rock chemical composition. Representative analyses are given in Appendix 1.

Regional Variations

Strong west-to-east and north-to-south gradients in the compositions of plutonic rocks are an important geochemical feature of the California batholiths and the calc-alkaline magmatic arcs of continental margins in general (see Dickinson, 1970; Kistler and Peterman, 1973; Kistler, 1974b, p. 416). Although latitudinal variations in whole-rock chemistry across the SNB and PRB, such as the well-defined west-to-east increases in K_2O, have been documented previously (Bateman and Dodge, 1970; Silver and others, 1979), we present these variations in the context of mafic silicate geochemistry and, in addition, show the effect of the little-studied western I-SCR types and eastern I-WC types on regional profiles. The positions of our west-to-east geochemical traverses A–A′ and B–B′ are shown in Figure 3B.

In A–A′, which extends across the Yosemite Valley, the west-to-east increase in F/OH in biotite at this latitude discussed by Ague and Brimhall (1987) is immediately apparent (Fig. 4). Covarying with F/OH in biotite are whole-rock SiO_2, K_2O, Rb/Sr, and molar $Al_2O_3/(CaO + K_2O + Na_2O)$, whereas CaO and MgO show a pronounced west-to-east decrease. Although $\log(X_{Mg}/X_{Fe})$ in biotite remains more or less constant at a value of approximately 0.0 (equal mole fractions of Mg and Fe) from west to east, molar whole-rock $MgO/(MgO + FeO)$ shows a pronounced decrease in the I-SC types due to the presence of abundant accessory magnetite correlating with the eastward increase in Fe_2O_3 documented by Dodge (1972). Molar $MnO/(MnO + TiO_2 + FeO + MgO)$ shows a marked increase in the I-SC types, which correlates with increases in X_{Mn} in biotite (see below). Cr is most abundant in the least evolved western I-WC types.

In contrast to the relatively smooth, generally monotonic regional variations documented in traverse A–A′, traverse B–B′, which extends across the central SNB, is considerably more complex, owing to the presence of the I-SCR belt and eastern I-WC types (Figs. 3, 4). The geochemical characteristics associated with the west-to-east progression from I-WC to I-SC types are broadly similar to those in traverse A–A′, but in the central portion of B–B′, these trends are locally disrupted by the siliceous I-SCR granites. Note in particular the high values of $Al_2O_3/(CaO + K_2O + Na_2O)$, largely due to the presence of magmatic muscovite, and high K_2O due to abundant microcline. The values of $\log(X_{Mg}/X_{Fe})$ and $\log(X_F/X_{OH})$ (in biotite) and whole-rock molar $MgO/(MgO + FeO)$ and molar $MnO/(MnO + TiO_2 + FeO + MgO)$ also attain extremes in the I-SCR types. In addition to the western occurrences, traverse B–B′ illustrates that I-WC types may also be present in the eastern SNB (sample 1011-16; Fig. 4). Note in particular the high Cr content of 91 ppm in sample 1011-16.

Major-, Minor-, and Trace-Element Systematics

With the regional variations in pluton chemistry in mind, we now examine key whole-rock geochemical parameters in order both to characterize the various pluton types more fully and to compare the compositional systematics of the California batholiths with the Australian I-, S-, and A-types and the magnetite and ilmenite series of Japan.

A plot of CaO versus SiO_2 (Fig. 5A) shows a smooth linear trend which grades from I-WC to I-SC and I-SCR types with increasing silica and decreasing CaO. This type of linear array is characteristic of I-type plutons worldwide (Czamanske and others, 1981). The plot of K_2O versus SiO_2 (Fig. 5B), however, while showing a general positive correlation, displays considerable scatter, with the I-SC and I-SCR types in general having the highest K_2O content. Figure 5C shows molar $Al_2O_3/(CaO + K_2O + Na_2O)$ versus SiO_2, and here, it is apparent that I-WC, I-MC, and I-SC types range in composition from metaluminous to weakly peraluminous. I-SCR types, in contrast, range from metaluminous to strongly peraluminous granites with molar $Al_2O_3/(CaO + K_2O + Na_2O)$ greater than 1.05. This reflects the fact that the I-WC, I-MC, and I-SC samples contain biotite as the most peraluminous phase whereas muscovite is present in the most peraluminous of the analyzed I-SCR samples. Values of molar $Al_2O_3/(CaO + K_2O + Na_2O)$ greater than 1.05 are characteristic of the S-types of Australia (White and Chappell, 1983). Na_2O shows no distinct variation between types (Fig. 5D), and it is important to note that none of the analyzed samples display the low Na_2O characteristic of the Australian S-types and most contain more Na_2O than does the average Australian I-type (White and Chappell, 1983).

Relationships between whole-rock MgO, FeO, MnO, and TiO_2 are important in the context of mafic silicate chemical systematics in that Mg, Fe, Mn, and Ti substitute into the octahedral sites of ferromagnesian minerals. Figure 5E illustrates that on average, the I-SCR types are the most magnesium poor although some I-SC granites are equally iron rich. The I-SC and I-SCR fields overlap, owing to the fact that we show all Fe as FeO. The I-SC types contain MgO-rich silicates and substantial magnetite (App. 2). The I-SCR types, on the other hand, generally contain minor ilmenite with Fe^{2+} being concentrated in the mafic phases. We note that values for average molar $MgO/(MgO + FeO)$ for Australian I- and S-types, 0.46 and 0.45, respectively, are comparable to those for I-WC, I-MC, and some I-SC types but are much higher than those of the I-SCR granites.

Although MnO decreases with SiO_2 content (App. 1), Figure 5F shows that molar $MnO/(MnO + TiO_2 + FeO + MgO)$ increases as silica increases, with the I-SC and I-SCR types displaying the highest degrees of relative Mn enrichment. This is consistent with available evidence regarding the behavior of Mn in magmatic systems. As pointed out by Goldschmidt (1954), magmas tend to have increasing $Mn/(Mg + Fe)$ with increasing differentiation, owing to the large ionic radius of Mn^{2+} and its consequent behavior as a relatively incompatible element. In addition, Hildreth (1979) has suggested that Mn may be concentrated in silicic magmas through some as yet poorly understood process of liquid-state differentiation. As Mn, Ti, Mg, and Fe are the primary substitutional metals in mafic mineral octahedral sites, this relationship indicates that the I-SC and I-SCR silicates should contain more Mn than those found in

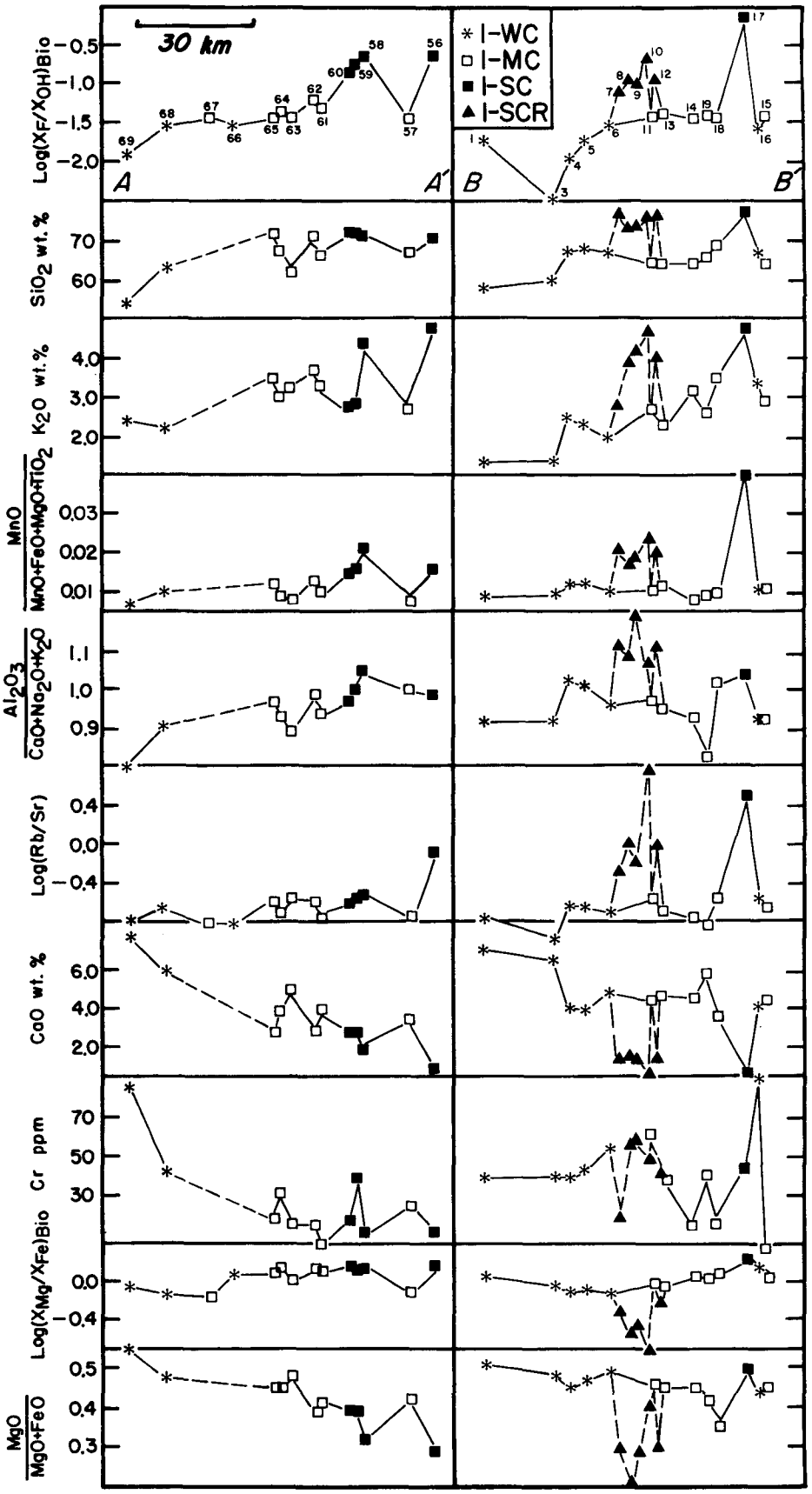

Figure 4. Geochemical traverses A–A′ and B–B′ (locations shown in Fig. 3B). Note relatively smooth west-to-east increases in incompatible elements and decreases in compatible elements in A–A′ corresponding to I-WC to I-SC progression. In B–B′, these trends are disrupted by geochemically distinct granites of the I-SCR belt. Note in particular the high values (as much as 1.18) of molar $Al_2O_3/(CaO + Na_2O + K_2O)$ in some I-SCR types and high Cr in I-WC–type 1011-16 in eastern SNB. All data are for whole-rock compositions except $\log(X_F/X_{OH})$ and $\log(X_{Mg}/X_{Fe})$, which are for biotites. $MnO/(MnO + FeO + MgO + TiO_2)$, $Al_2O_3/(CaO + Na_2O + K_2O)$, and $MgO/(MgO + FeO)$ are molar ratios. Whole-rock major oxides and minor elements were not analyzed for samples 66 and 67 of A–A′. Other reports containing analytical data and geologic mapping for A–A′ to which our results may be compared include Kistler (1966), Bateman and others (1983) (samples 1011-56 through -57); Bateman and Chappell (1979), Reid and others (1983), Kistler and others (1986) (samples 1011-58 through -60); and Kistler (1973, 1974a) (samples 1011-61 through -65).

I-WC and I-MC types. Increased Mn would also be expected in both I-SC– and I-SCR–type ilmenites.

The distribution of selected trace elements and elemental ratios is displayed in Figure 6. Rb/Sr increases from I-WC to I-SC types, with the I-SCR types having the highest average values (Fig. 6A). In contrast, Cu and Zn are concentrated in the I-WC and I-MC types (Figs. 6B, 6C). Cr attains high values in both mafic I-WC and I-MC types and in some I-SCR samples, whereas the I-SC types contain on average the lowest Cr (Fig. 6D). In general, the I-SC and I-SCR types are the most enriched in incompatible elements such as Rb, Th, and Nb, whereas more compatible elements such as Ni are concentrated in the more mafic I-WC and I-MC types (App. 1).

Bulk chemical data indicate that although some I-SCR types can be markedly peraluminous, the analyzed intrusives display predominantly "I-type" characteristics as defined by White and Chappell (1983) and White and others (1986), with the I-WC types being in general the most mafic and the I-SC and I-SCR types being the most felsic. Some I-SCR samples, however, may have the high SiO_2 and Na_2O

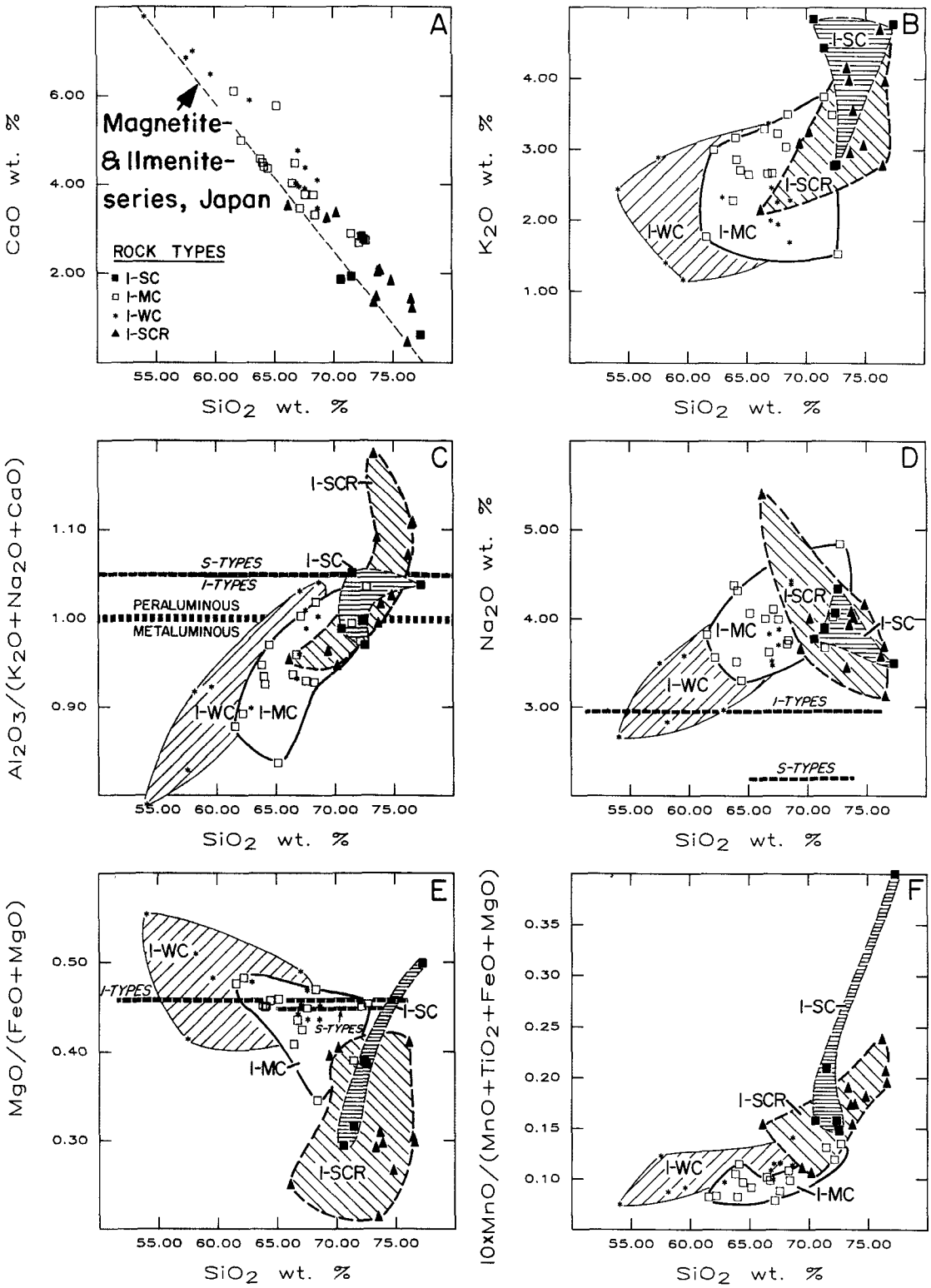

Figure 5. Whole-rock geochemical systematics based on XRF analyses of 44 samples. A. CaO versus SiO_2. Note similarity to trend defined by Japanese magnetite- and ilmenite-series plutons. B. K_2O versus SiO_2. C. Molar $Al_2O_3/(CaO + Na_2O + K_2O)$ versus SiO_2. Only I-SCR types display the "S-type" characteristic of $Al_2O_3/(CaO + Na_2O + K_2O) > 1.05$. D. Na_2O versus SiO_2. The California batholiths are generally more Na_2O rich than are both average Australian I-types ($Na_2O = 2.95$) and S-types ($Na_2O = 2.2$). E. Molar $MgO/(MgO + FeO)$ versus SiO_2. Note that I-SCR types are in general the most Mg poor, with $MgO/(MgO + FeO)$ lower than in both average Australian I-types and S-types [$MgO/(MgO + FeO) = 0.46$ and 0.45, respectively]. F. $10 \times MnO/(MnO + FeO + MgO + TiO_2)$ (moles) versus SiO_2. I-SC and I-SCR types are in general more Mn enriched, relative to Fe, Ti, and Mg, than are I-WC and I-MC types. Data for the magnetite and ilmenite series are from Czamanske and others (1981); data for I-types and S-types are from White and Chappell (1983).

and low Al_2O_3 characteristic of minimum melts (White and Chappell, 1977) (App. 1, sample 12), possibly indicating a local anatectic origin. The high values of Cr in the more mafic I-WC and I-MC types reflect the compatible nature of this element, whereas high Cr in some I-SCR granites (as much as 60 ppm) may indicate the involvement of marine sedimentary source materials as Cr may be concentrated into clays during weathering (White and Chappell, 1983). The compatible element Ni is concentrated into the more mafic I-WC and I-MC samples, however, and shows no enrichment in the I-SCR types, in contrast to the high Ni values (average 17 ppm) reported for the Australian S-types

(White and Chappell, 1983). The distinctively high Ga/Al and Zr of A-type granites (average Ga/Al = 4.0, Zr = 554 ppm; Collins and others, 1982; Whalen and others, 1986) does not find a parallel in any of the 114 samples we have analyzed (App. 1).

MINERALOGY

On the basis of the whole-rock geochemical systematics presented above, it follows directly that the compositions of mafic silicates are broadly correlative with host rock lithology. In general, the most mafic rocks fall within the I-WC group, whereas the most siliceous rocks are of I-SC or I-SCR type (Fig. 7). Accessory mineral assemblages also correlate with mafic-phase chemical characteristics and rock type. Modes for 20 representative samples are given in Appendix 2.

I-WC types range in composition from quartz diorite to granodiorite, and color indices vary between 16 and 50. The vast majority of samples contain plagioclase, quartz, orthoclase, amphibole, and biotite with or without pyroxene, magnetite, ilmenite, and sphene (Figs. 7, 8A, and 8B). Color indices of I-MC types are lower than for I-WC types and vary from 6 to 35. The I-MC and I-WC types are similar in that they generally contain hornblende, except in the San Gabriel Mountains where amphibole is in many cases absent (Fig 8B). Pyroxene is absent from I-MC types, however, and the rocks typically range in composition from granodiorite to granite, although some I-MC types, such as those from the San Jacinto Mountains of the PRB, may be tonalitic (Hill and others, 1986). In the I-SC types, amphibole is absent from 76% of the samples, and the rocks range from quartz monzonite to granite in composition. Color indices are low compared to both the I-WC and I-MC types and range from 2 to 9. In contrast to the I-WC and I-MC types, which generally contain orthoclase, I-SC types may have substantial microcline. Nonreplacive muscovite is present in an I-SC type from the central SBB, and muscovite and subhedral garnet coexist in a small I-SC intrusive from the northern SNB in the metamorphic foothills belt.

Figure 8C shows that primary sphene-bearing assemblages are virtually restricted to I-WC, I-MC, and I-SC types. Samples containing only alteration sphene produced by the loss of Ti from magnetite during cooling or the chloritization of biotite are not categorized as "sphene-bearing" as this sphene is not indicative of magmatic conditions. Petrographic observations indicate that the majority of the I-WC, I-MC, and I-SC types are of Ishihara's (1977) magnetite series, although some I-WC and, to a much

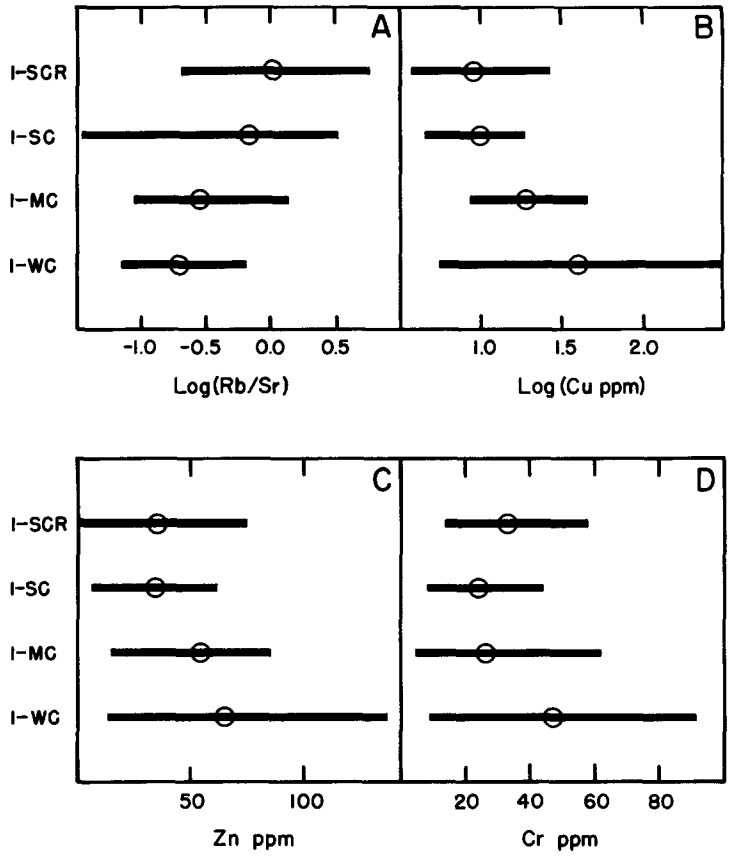

Figure 6. Trace-element systematics. Circles indicate average values. In general, I-SCR and I-SC types are enriched in the incompatible element Rb, whereas I-WC and I-MC types contain higher concentrations of compatible elements. Figures are based on 114 analyses for Rb, Sr, Zn, and Cu and on 44 analyses for Cr. A. Log(Rb/Sr). B. Log(Cu parts per million). C. Zn parts per million. D. Cr parts per million. Note that I-SCR types can contain high Cr of as much as 60 ppm.

Figure 7. QAP diagram (I.U.G.S. rock names) showing broad correlations between biotite chemistry and modal mineralogy. I-WC and I-MC types are generally the most mafic, whereas I-SCR and I-SC types are typically "true" granites in terms of modal mineralogy.

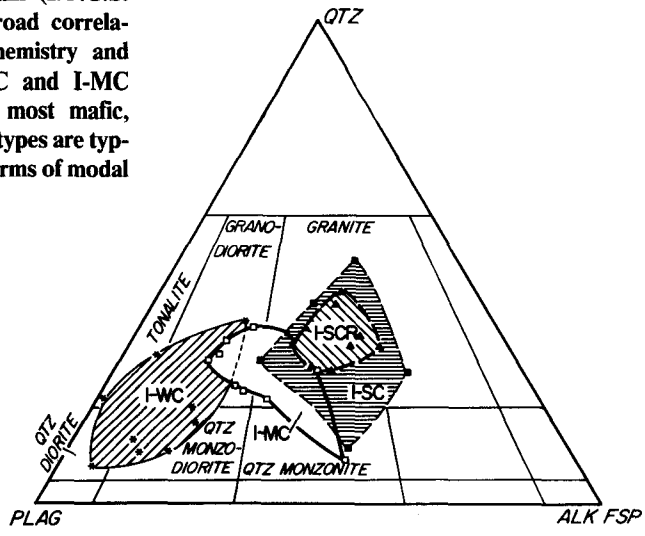

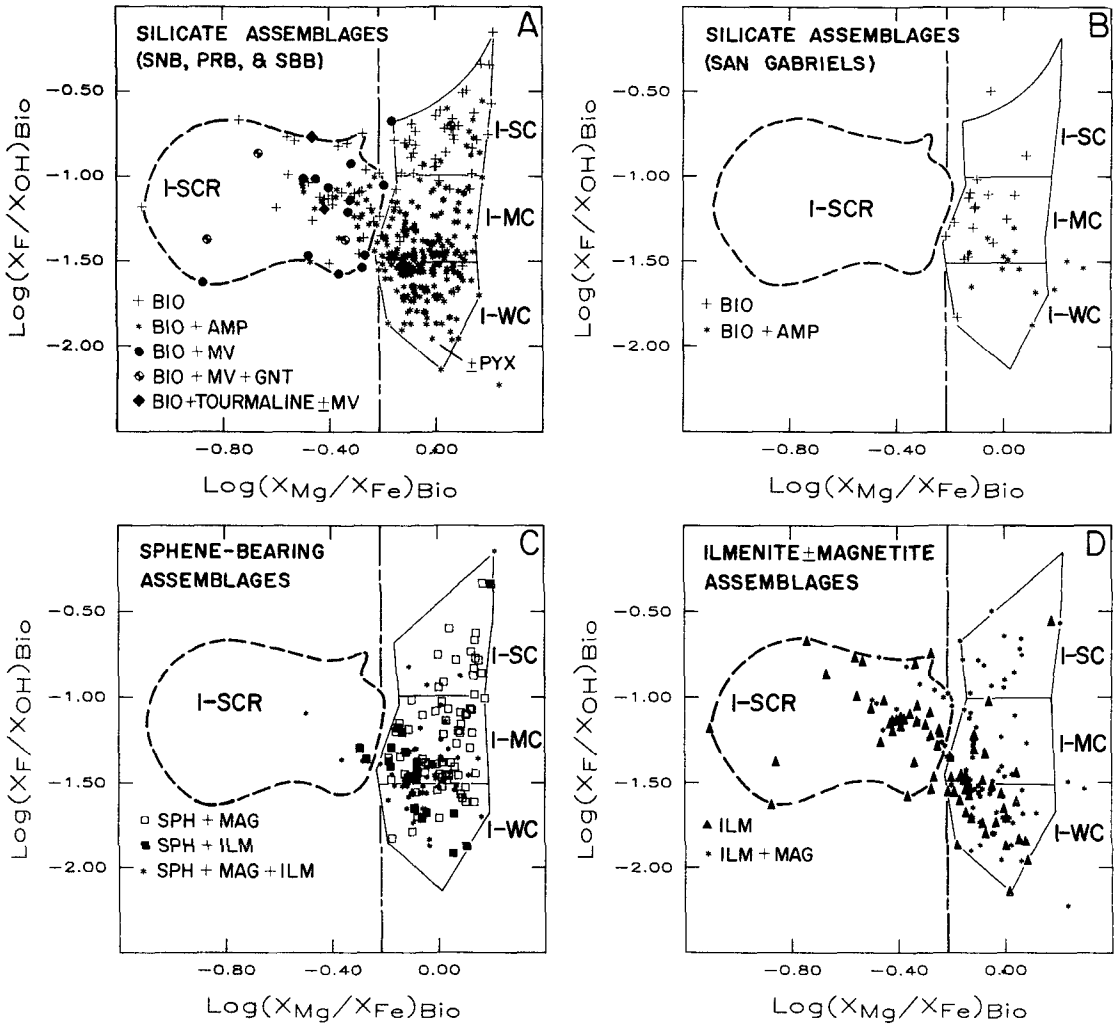

Figure 8. Coexisting mineral assemblages in relation to biotite chemistry. A. Biotite compositions for the SNB, PRB, and SBB. Note abundance of aluminous minerals in the I-SCR group. B. Biotite compositions for the SGB. Note absence of I-SCR types. C. Primary sphene-bearing assemblages for all batholiths. Sphene only rarely coexists with I-SCR-type biotites. D. Ilmenite + magnetite assemblages.

lesser degree, I-MC and I-SC types belong to the ilmenite series (Figs. 8C, 8D).

I-SCR types comprise a wide variety of assemblages and mineralogically are typically true granites with low color indices ranging from 2 to 16. The majority of I-SCR types contain microcline, quartz, plagioclase, biotite, and ilmenite, with or without magnetite. Other minerals which may occur include amphibole, garnet, muscovite, and tourmaline (Fig. 8A). Cordierite has not been found in any of the studied samples. Amphibole is present in only 30% of the specimens and never coexists with muscovite, garnet, or tourmaline. Allanite crystals may be associated with mafic phases and can attain 3 mm in length. Anhedral to subhedral zircon, and to a lesser degree monzonite, is commonly included within biotites and may represent refractory material inherited from sedimentary protoliths (compare with Sawka and others, 1986). Ilmenite alone or with magnetite is the predominant accessory assemblage, with primary sphene being extremely rare (Figs. 8C, 8D). Petrographic observations indicate that the bulk of the I-SCR types parallel Ishihara's (1977) ilmenite series, first defined for Japanese granitoids on the basis of iron-titanium oxide content and assemblages.

Sulfides are rare in the plutonic rocks of the batholiths; pyrrhotite, pyrite, and chalcopyrite have been observed either as anhedral, interstitial crystals or as inclusions within amphibole or magnetite. The occurrence of magnetite alone is not restricted to any particular rock type, although only 13% of the I-SCR types contain this assemblage.

Mafic inclusions, composed of plagioclase, amphibole, and biotite with or without K-feldspar, magnetite, ilmenite, and sphene, are common in the I-WC and I-MC types but are rare in I-SC granites. Microscopically, they are texturally distinctive in that late-formed microcline and biotite poikilitically enclose early-formed minerals such as plagioclase. In contrast, I-SCR types rarely contain mafic inclusions of any kind. The inclusions which do occur are typically small (on the order of 1 cm) aggregates of biotite or, less commonly, muscovite, biotite, and accessory phases.

Although biotite is present in nearly all of the unaltered specimens studied, monzonites from the Joshua flat pluton of the White-Inyo Mountains (Sylvester and others, 1978), the granodiorites of the Strawberry W Mine of the SNB (Nokleberg, 1981), and uncommon mafic and intermediate rocks from the SGB and western SNB and PRB lack biotite but contain amphibole with or without pyroxene, magnetite, sphene, and ilmenite.

I-SCR types may occur as discrete plutons (for example, granite of Shuteye Peak; Stern and others, 1981) or as granite facies of compositionally variable plutons such as the Bonsall Tonalite described by Larsen (1948). In general, plutons which are compositionally variable, such as the Mount Givens granodiorite (Stern and others, 1981), which ranges from I-MC to I-SC type, may comprise more than one rock type as defined herein on the basis of biotite chemistry.

MINERAL CHEMISTRY

In order to understand rigorously the implications of pronounced spatial variations in mineral chemistry and petrology which exist in the California batholiths, it is essential to examine the compositional systematics of mafic silicates and accessory minerals and to assess the preservation of equilibrium between plutonic biotites and amphiboles. Our discussion is based upon microprobe analyses of biotites in 376 samples, amphiboles in 287 samples, garnets in 4 samples, sphenes in 103 samples, magnetites in 94 samples, and ilmenites in 107 samples.

The Fe^{3+} content of amphibole can be significant, and therefore, we have estimated the ferrous iron content of the analyzed specimens using the procedure discussed by Stout (1971) and Brady (1974). Because large and unsystematic errors may occur when estimating biotite Fe^{3+} content, we have calculated biotite structural formulas taking all Fe as FeO. Ilmenite and magnetite formulas were derived using the procedures of Carmichael (1967).

X_F, X_{Cl}, and X_{OH} have been calculated assuming two structural water sites in amphibole and biotite. Because natural biotites and amphiboles in many cases show an anion site deficiency, this method tends to overestimate X_{OH} slightly. The error in log (X_F/X_{OH}) in biotites is typically small, however, and is generally in the range of 0.05 to 0.1 log units (Munoz, 1984).

Biotite Chemistry

$Log(X_{Mg}/X_{Fe})$ ranges from –1.105 to 0.298 in the analyzed biotites. There is generally no systematic Mg/Fe zonation within individual crystals, although Mg- and Al-enriched biotite rims have been noted in several samples. Biotite $log(X_{Mg}/X_{Fe})$ and total Al are shown in relation to coexisting phase assemblages in Figure 9. Although the biotites cover a wide range of the compositional field, it is clear that the biotites that have the lowest Al have the highest Mg/Fe whereas the most Al-enriched specimens tend to be low Mg/Fe I-SCR types. From Figure 9, it is evident that the presence of aluminous minerals such as muscovite and garnet fixes coexisting biotite aluminum content at high values, typically greater than 1.55 formula units (f.u.).

Mn also varies widely in the analyzed biotites, with Mn ranging from 0.004 to 0.141 f.u. Figure 10A shows that the I-SC and I-SCR biotites tend to be the most Mn rich. If the evidence from the whole-rock chemistry section presented earlier, which illustrated the general increase in $MnO/(MnO + FeO + MgO + TiO_2)$ with increasing SiO_2, is used, the generally higher Mn in I-SC and I-SCR granite biotites may be explained in terms of high $MnO/(MnO + FeO + MgO + TiO_2)$ in the bulk rock composition.

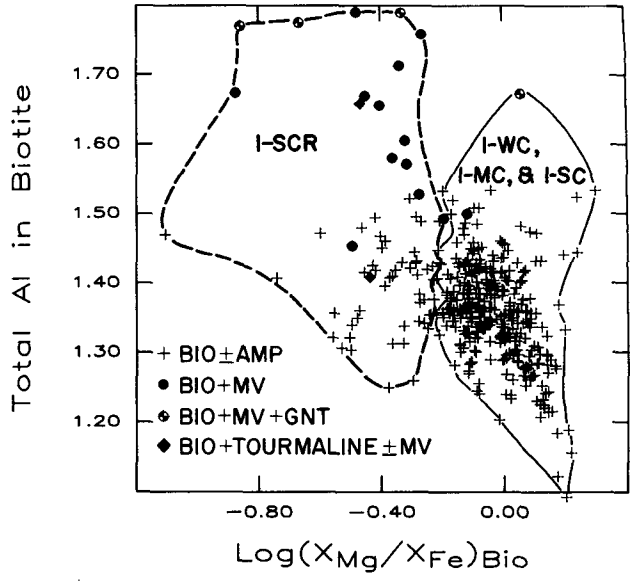

Figure 9. Total Al (formula units) versus $log(X_{Mg}/X_{Fe})$ for biotite. The most Al-rich biotites (total Al > 1.55) typically have $log(X_{Mg}/X_{Fe}) < -0.21$ and always coexist with an aluminous phase such as muscovite, garnet, or tourmaline.

F and Cl contents range from 0.005 to 0.828 f.u. and <0.001 to 0.06 f.u., respectively. Figure 10B shows that there is overlap between I-WC, I-MC, and I-SC types in $log(X_F/X_{Cl})$, but the relationships evident in Figure 3A using $log(X_F/X_{OH})$ still are present. Within the limits of detection, the halogens are unzoned within the biotites. Figures 10C and 10D show X_{Cl} and X_F versus X_{Mg}, and here, it is apparent that in contrast to numerous examples of micas from hydrothermal ore deposits (Jacobs and Parry, 1979; Gunow and others, 1980; Munoz and Swenson, 1981; Munoz, 1984; Brimhall and others, 1985), positive linear correlations between X_F and X_{Mg} and negative correlations between X_{Cl} and X_{Mg} are not present for these plutonic biotites. Because the linear arrays defined by hydrothermal biotite compositions are interpreted to represent isotherms (Munoz and Swenson, 1981; Brimhall and Ague, 1988), it is not surprising that the plutonic biotites do not form such arrays, owing to the wide ranges in crystallization temperature and magmatic volatile fugacities in the plutonic environment. In general, owing to Fe-F and Mg-Cl avoidance (Munoz, 1984), the highest F contents are found in the more magnesian biotites, whereas Fe-rich I-SCR biotites contain the most Cl. It is significant to note at this point, however, that Fe-rich I-SCR biotites may be relatively high in F, and Mg-rich biotites may contain substantial Cl (Figs. 10C, 10D).

Ti contents vary from 0.037 to 0.280 f.u. and show no obvious correlation with rock type. The presence of rutile needles and/or alteration sphene in a large number of samples, however, suggests that the biotites have not retained their original high-temperature Ti signature. Ti may in some cases be lower on the rims of biotite grains, and this also probably reflects the decreasing solubility of Ti in mafic phases with decreases in temperature (for example, Anderson, 1980).

Amphibole Chemistry

The amphiboles fall in the compositional range between tremolite and pargasite, with the vast majority of samples having the composition of hornblende (Deer and others, 1966, p. 168–169). As is the case for biotite, $log(X_{Mg}/X_{Fe^{2+}})$ varies over a wide range in amphiboles from –0.542 to 0.420. Calculated Fe^{3+} contents show no evidence of a positive correlation between Fe^{3+} and total iron. The I-SCR amphiboles thus have lower Fe^{3+}/Fe^{2+} ratios than do those of the I-WC, I-MC, and I-SC types.

From the work of Hammarstrom and Zen (1986), it is likely that in granitic rocks, crystallization pressure strongly controls amphibole Al content. Figure 11A demonstrates that there is a good correlation between Al^{IV} and total Al similar to that displayed by the amphiboles used to calibrate the empirical hornblende geobarometer of Hammarstrom and Zen (1986).

The halogen contents covary with those of the biotites over a large interval, with F and Cl ranging from 0.005 to 0.8 f.u. and 0.001 to 0.08 f.u., respectively. As is the case for biotite, the halogens show no systematic zonation. In the $log(X_F/X_{OH})$ versus $log(X_{Mg}/X_{Fe^{2+}})$ coordinate system, amphiboles from the different rock types occupy distinct compositional fields with a minimum of overlap (Fig. 11B).

Mn ranges from 0.031 to 0.260 f.u. and, as is the case for biotites, attains the highest values in I-SC and I-SCR types. Amphibole Ti contents show no variation with type and range from 0.040 to 0.227 f.u. Exsolution of *titanium in*

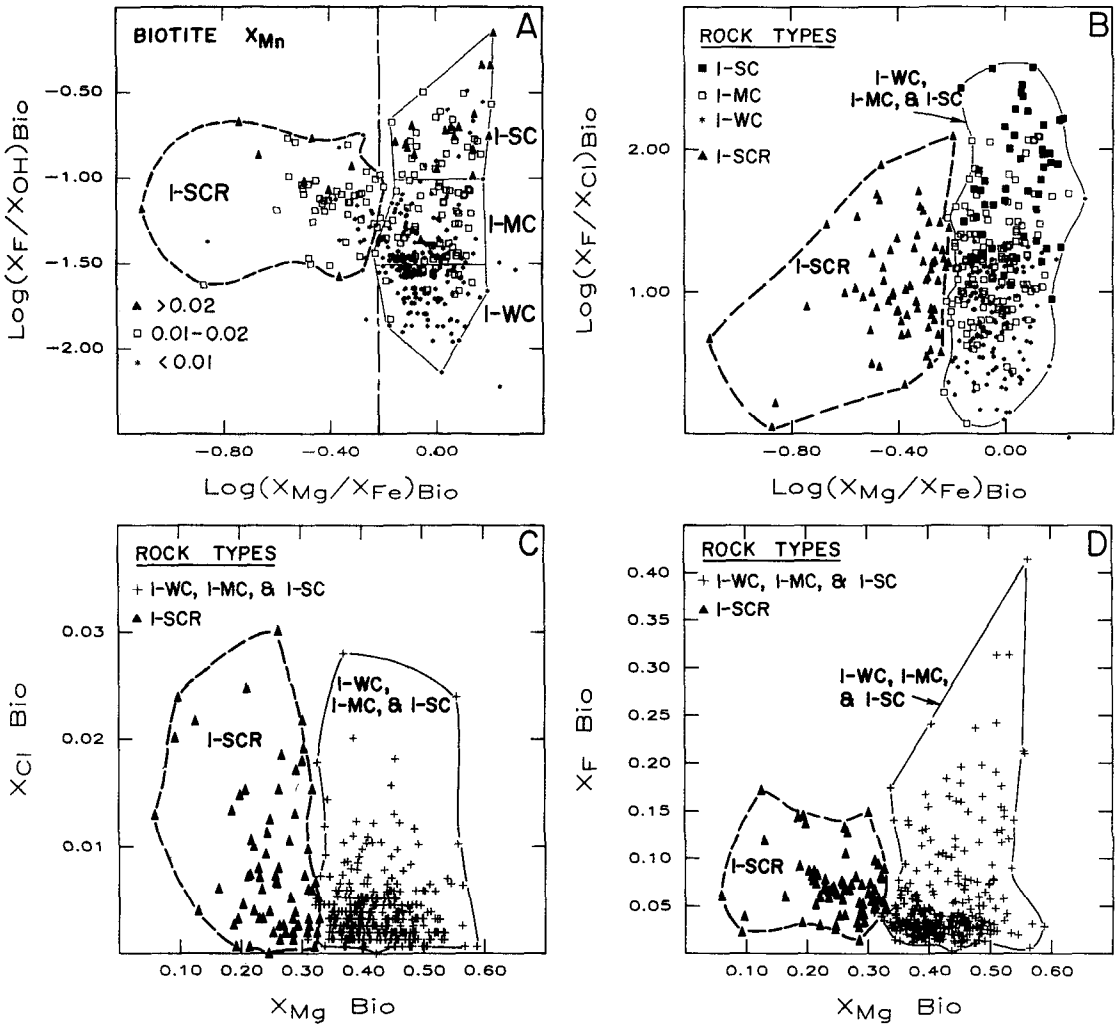

Figure 10. Biotite compositional systematics. A. X_{Mn} in biotite. In general, I-SC- and I-SCR-type biotites are the most Mn rich. B. Log(X_F/X_{Cl}) versus log(X_{Mg}/X_{Fe}). C. X_{Cl} versus X_{Mg}. D. X_F versus X_{Mg}.

amphibole in the form of sphene or rutile has not been observed in any of the studied samples, and it is therefore probable that unlike biotite, the amphibole compositions record a high-temperature magmatic signature for Ti.

Elemental Partitioning between Mafic Phases

It is important to evaluate geochemical interrelationships between coexisting amphiboles and biotites in order to ascertain the preservation of equilibrium and the possible temperature dependency of elemental partitioning between these phases.

Figure 12A shows log($X_{Mg}/X_{Fe_{total}}$) for coexisting amphiboles and biotites from the batho-

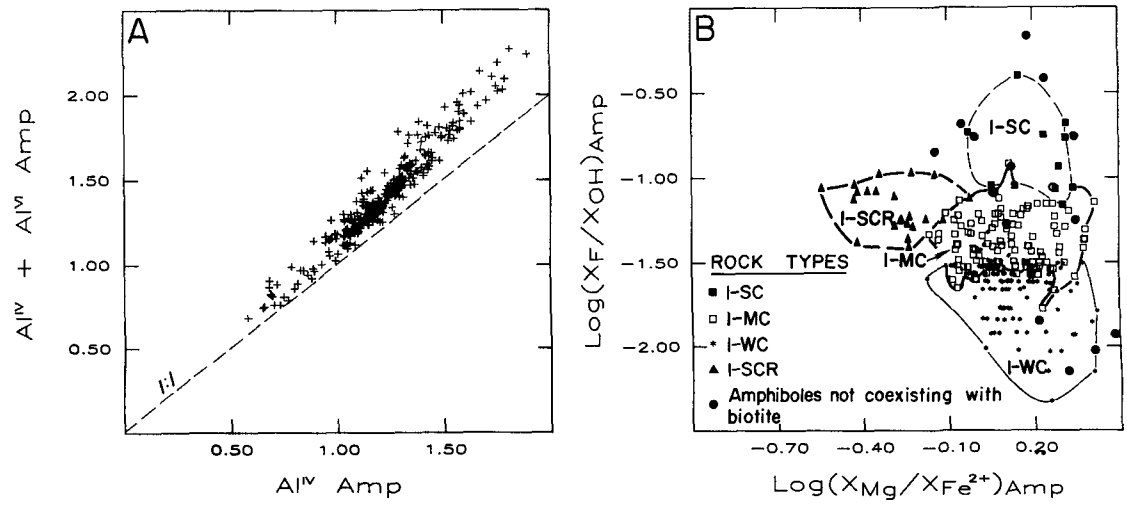

Figure 11. Amphibole compositional systematics. A. Total Al versus Al^{IV} (all rock types). Note covariation of Al^{VI} and Al^{IV}. B. Log(X_F/X_{OH}) versus log($X_{Mg}/X_{Fe^{2+}}$). Amphiboles from I-WC, I-MC, I-SC, and I-SCR types occupy distinct compositional fields with only minor overlap.

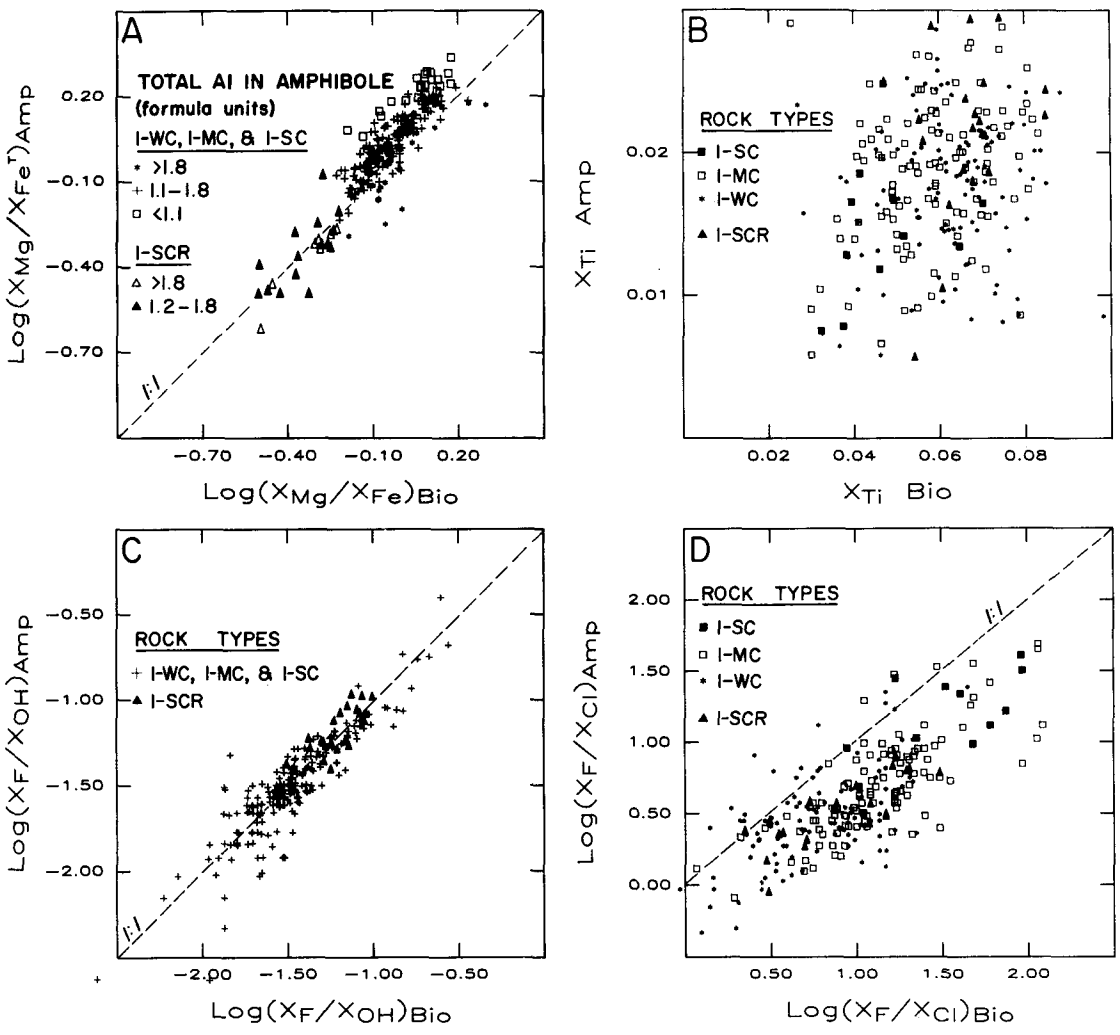

Figure 12. Partitioning of elements between biotite and amphibole. A. $Log(X_{Mg}/X_{Fe})$ (all Fe as FeO) in amphibole versus $log(X_{Mg}/X_{Fe})$ in biotite showing dependence of partitioning of Fe and Mg between biotite and amphibole on amphibole Al content. B. X_{Ti} in amphibole versus X_{Ti} in biotite. Note lack of systematic partitioning of Ti between coexisting mafic phases. C. $Log(X_F/X_{OH})$ in amphibole versus $log(X_F/X_{OH})$ in biotite, showing excellent positive correlation. D. $Log(X_F/X_{Cl})$ in amphibole versus $log(X_F/X_{Cl})$ in biotite. In general, amphiboles contain more Cl than do coexisting biotites.

liths studied. The distribution of data points is quite linear and shows a slight preference of amphibole for Mg, with the least aluminous amphiboles showing the greatest preference for Mg. The Ti distribution is shown in Figure 12B. There is almost no correlation between amphibole and biotite Ti contents, which probably reflects low-temperature subsolidus re-equilibration, as deduced elsewhere (Czamanske and others, 1981).

$Log(X_F/X_{OH})$ shows an excellent positive correlation for coexisting biotite and amphibole (Fig. 12C). No systematic preference of biotite or amphibole for F is evident from our analyses. $Log(X_F/X_{Cl})$ is also positively correlated between biotites and amphiboles, showing a preference of amphibole for Cl, although some scatter is present (Fig. 12D).

We conclude that the octahedrally coordinated cations Mg and Fe, and the anions F, Cl, and OH, preserve high-temperature equilibrium relationships. The scatter in the distributions may be due to minor disequilibrium, temperature dependence of the exchange reactions, or analytical error. Ti does not display a high-temperature distribution between mafic phases, owing to probable subsolidus re-equilibration.

Garnet and Sphene Chemistry

Garnets in I-SCR types are dominated by the almandine component, but appreciable spessartine may also occur in solid solution. The high X_{Mn} (as much as 0.47) in the garnets from samples 1011-303, -418, and -423 is typical of igneous garnets (Miller and Stoddard, 1981) and may reflect crystallization in response to high Mn/(Mn + Fe) in differentiated magmas.

We have analyzed sphene for the major oxides and halogens but not REE's, Nb, Ta, or V. The sphenes are all similar with respect to their major-element chemistry, with primary grains containing as much as 3 wt.% Fe_2O_3 and 2.5 wt.% Al_2O_3. Sphene in sample 1011-200, which is intergrown with chlorite and represents an alteration product of biotite, contains 5.97 wt.% Al_2O_3. The fluorine content of sphene correlates well with that of coexisting mafic silicates and increases systematically from I-WC to I-SC types.

Magnetite Chemistry

Of 94 analyzed magnetites from rocks of all types, only 1 sample from the San Gabriel Mountains (1011-165) appears to have retained its primary Ti content. In addition, several samples from the southwestern PRB and western SBB contain magnetite with variable TiO_2 contents less than 4 wt.%. The vast majority of the magnetites, however, typically contain less than 0.3 wt.% TiO_2 and small amounts of MnO, Al_2O_3, and MgO. The presence of nearly pure Fe_3O_4 in granitic rocks is very common (compare with Noyes and others, 1983) and reflects the loss of Ti, either through exchange with mafic silicates or by the formation of a secondary Ti-rich mineral such as sphene, from magnetite during slow cooling.

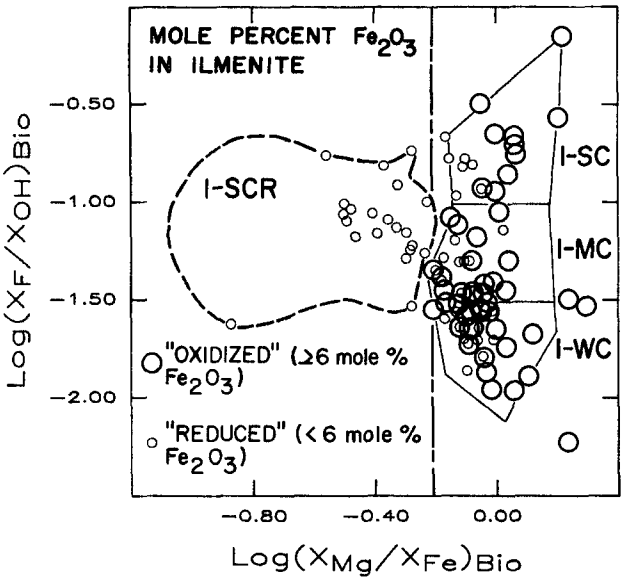

Figure 13. Ilmenite Fe_2O_3 mole percent plotted in terms of coexisting biotite composition. Note that "reduced" ilmenites with $Fe_2O_3 < 6$ mole percent are present in I-SCR types. "Oxidized" ilmenites containing 6 mole percent or more Fe_2O_3 are common in the I-WC, I-MC, and I-SC types.

Ilmenite Chemistry

Ilmenite occurs in rocks of all types studied and varies substantially in Fe_2O_3 and MnO. Figure 13 shows that calculated maximum mole percent Fe_2O_3 for I-WC, I-MC, and I-SC types may exceed 6 mole % (reaching a maximum of 20 mole %), whereas ilmenites from I-SCR types have less than 6 mole % hematite. As in biotites and amphiboles, Mn content is highest in the ilmenites from I-SC and I-SCR types. I-SCR ilmenites are generally homogeneous in reflected light, but I-WC, I-MC, and I-SC ilmenites may display micron-scale exsolution features. Grains with significant exsolution were analyzed with a wide (10 μ) microprobe beam. In contrast to Czamanske and others (1981), separate ilmenites from a single sample do not show significant compositional variation.

REGIONAL VARIATIONS

We now examine in detail previously unrecognized spatial variations in mineral assemblages and mafic mineral chemistry in the California batholiths. These variations are of central importance in understanding geologic factors controlling intrusive chemistry and the evolution of batholiths at convergent plate boundaries where magmas derived from downgoing subducted slabs, the upper mantle, or crust may interact with a diverse array of geochemically distinct pre-batholithic terranes.

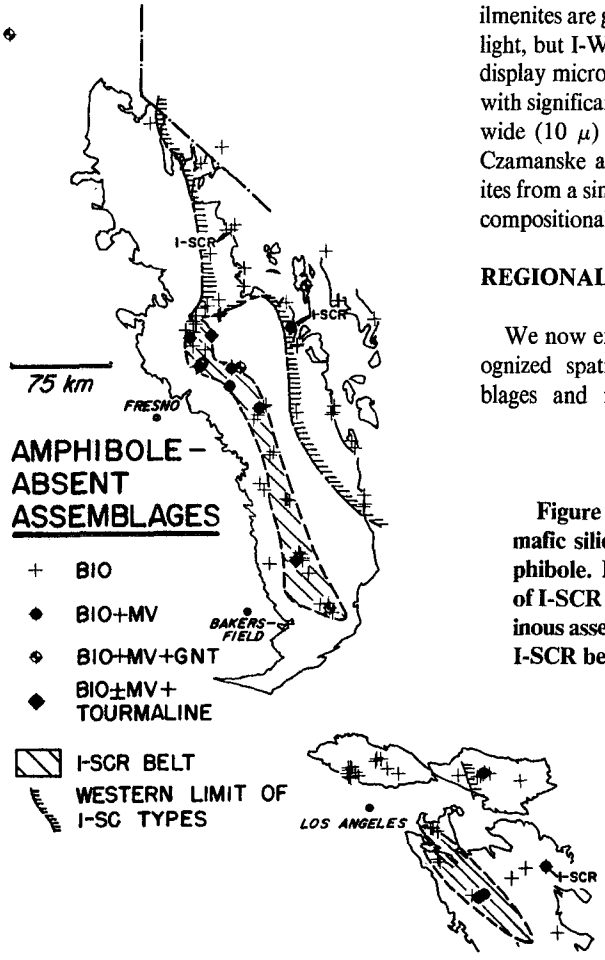

Figure 14. Regional distribution of mafic silicate assemblages lacking amphibole. Biotite granites are generally of I-SCR or I-SC type. Note that aluminous assemblages typically occur within I-SCR belts.

Mineral Assemblages

One of the most useful petrologic distinctions between I-SC and I-SCR granites and the more mafic I-WC and I-MC types is the general absence of amphibole in the I-SC and I-SCR types. Although the assemblage biotite + amphibole is widespread, granitic rocks with biotite but no amphibole are prevalent in the eastern SNB and SBB and in narrow northwest-trending belts in the western SNB and PRB (Fig. 14). The eastern "biotite only" assemblages correspond in general to I-SC plutons, whereas the northwest-trending belts in the SNB and PRB are defined by I-SCR types. Also shown are the occurrences of the aluminous minerals muscovite, garnet, and tourmaline, and here, it is clear that these minerals typically occur in the I-SCR belts. The rocks of the SGB in many cases lack amphibole; here, however, the rocks are of I-MC or I-SC affinity. The SGB has been subjected to a complicated series of tectonic and metamorphic events (Ehlig, 1981), and it is therefore probable that the compositions of phases from the SGB may not always be directly comparable with those from the rest of the batholiths.

The regional distributions of accessory mineral assemblages define systematic variations which correlate with rock type and silicate character (Figs. 15A, 15B). The assemblages ilmenite or ilmenite + magnetite in both the SNB and PRB occur almost exclusively in the western portions of the batholiths, generally in rocks of I-SCR, I-WC, and I-MC type. These assemblages also occur within isolated I-SCR types from the eastern SNB and PRB, in I-SC types in the vicinity of the Strawberry W Mine, and in I-SC types of the SBB. The magnetite + ilmenite + sphene assemblage is found south of 38° N. latitude in the SNB, the western SBB, and throughout the PRB, generally within I-WC and I-MC types, although rare I-SC and I-SCR granites also contain this assemblage. The highly oxidized assemblage magnetite + sphene occurs in the northern and eastern SNB and eastern PRB, whereas the relatively uncommon assemblage ilmenite + sphene is present in the eastern PRB and sporadically in the SNB. We should emphasize at this point that the ilmenites in the I-SCR types define local-scale compositional discontinuities in regional ilmenite composi-

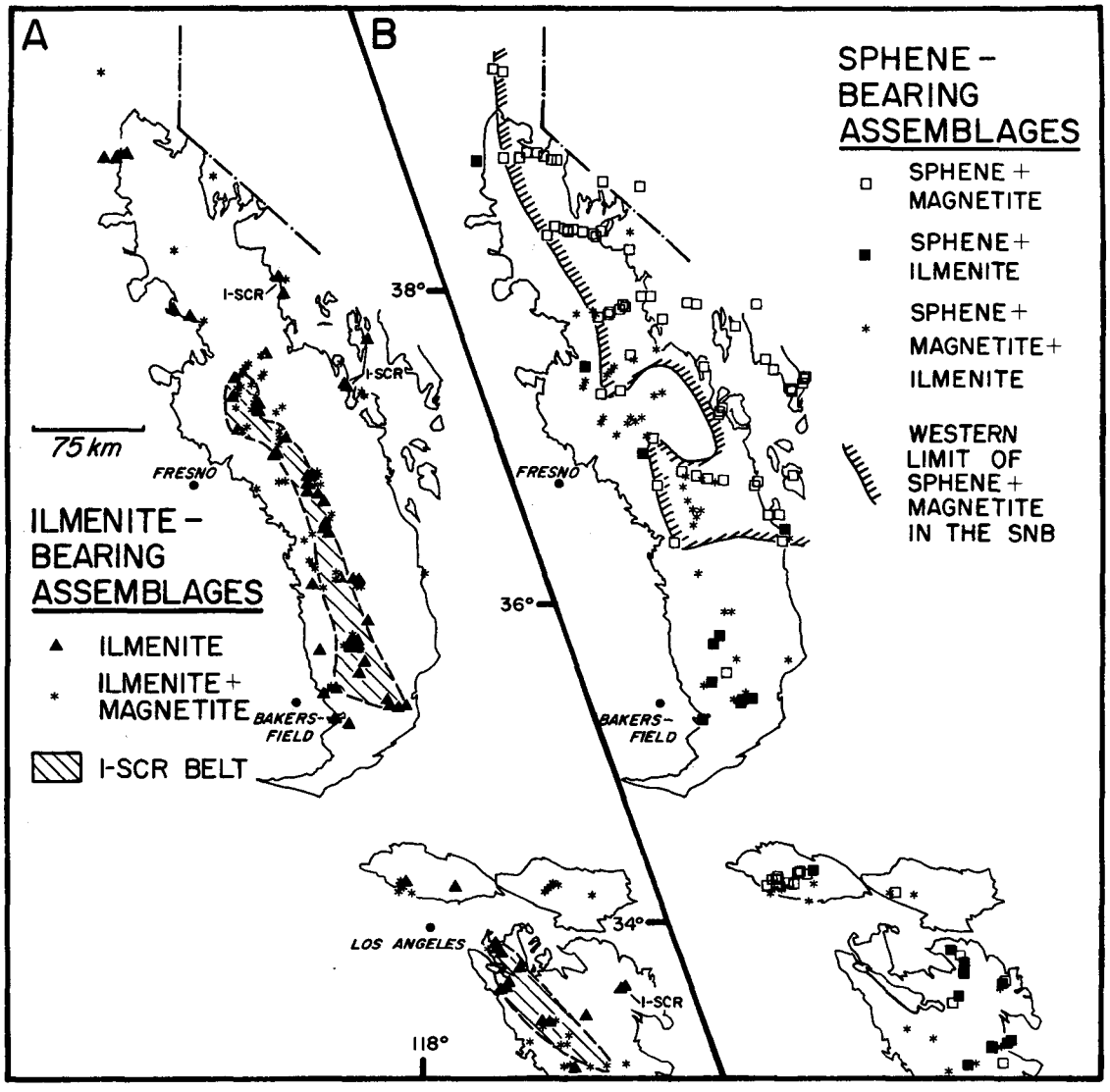

Figure 15. Regional distribution of accessory mineral assemblages. A. Ilmenite + magnetite. B. Sphene-bearing assemblages. Sphene + magnetite assemblages dominate in the northern and eastern SNB.

tional systematics as they are always "reduced" (containing less than 6 mole % Fe_2O_3), whereas ilmenites in I-WC, I-MC, and I-SC types may contain as much as 20 mole % Fe_2O_3.

We have purposely delayed discussion of the accessory minerals of the SGB to this point. Here, representatives of all the assemblage types discussed above are present, but their regional distribution is generally unsystematic, at least at the reconnaissance scale of sampling, although the magnetite + ilmenite assemblage is concentrated in the western portion of the range.

Mineral Chemistry

Because mafic silicate compositions relate to critical magmatic intensive variables in granitic systems, spatial variations in ferromagnesian mineral chemistry provide insight into the geochemical character of magmatic source components and pluton crystallization pressure. Here, we present surface contour plots of mafic silicate compositional parameters in order to elucidate regional geochemical systematics. Besides our own data, we have used several analyses of mafic silicates from Dodge and others (1968, 1969; samples KR, BCA-20, BCC-12, and BCC-13) as these specimens are from a region in the central SNB which we did not sample. In addition, unless otherwise noted, average values are shown for the SGB, owing to a small sample set and general lack of well-defined spatial variation.

The contoured surfaces are generated using Precision Visuals graphics computer subroutines for computing splines under tension, a three-dimensional curve-fitting process that produces smooth contour lines. The method of gridding uses an algorithm by Akima (1978), which uses the triangulation algorithm of Lawson (1977). The X-Y plane is divided into triangulation cells, each having projections of the 3-data points in the plane at its vertices. A bivariate fifth degree polynomial in X and Y is applied to interpolate points within the triangle. Estimated values of partial derivatives at each data point are used in determining the polynomial. No input data smoothing is performed, and the output gridded array passes through all the input points.

A truly remarkable and significant feature of the batholiths is the general west-to-east increase in the fluorine content of hydrous mafic silicates. In Figures 16A and 16B, we have contoured $\log(X_F/X_{OH})$ in biotites and amphiboles, respectively, for the I-WC, I-MC, and I-SC types. The I-SCR types show little or no systematic regional variation and, because they disrupt the regional F/OH systematics as shown previously in Figure 4, have been omitted for clarity. In the SNB and SBB, there are well-defined west-to-east increases in F/OH in mafic silicates, corresponding to the eastward progression from I-WC to I-MC and I-SC types. Figures 16A and 16B also demonstrate, however, that I-WC types may be present in the eastern SNB. The PRB shows west-to-east increases in F/OH, but here,

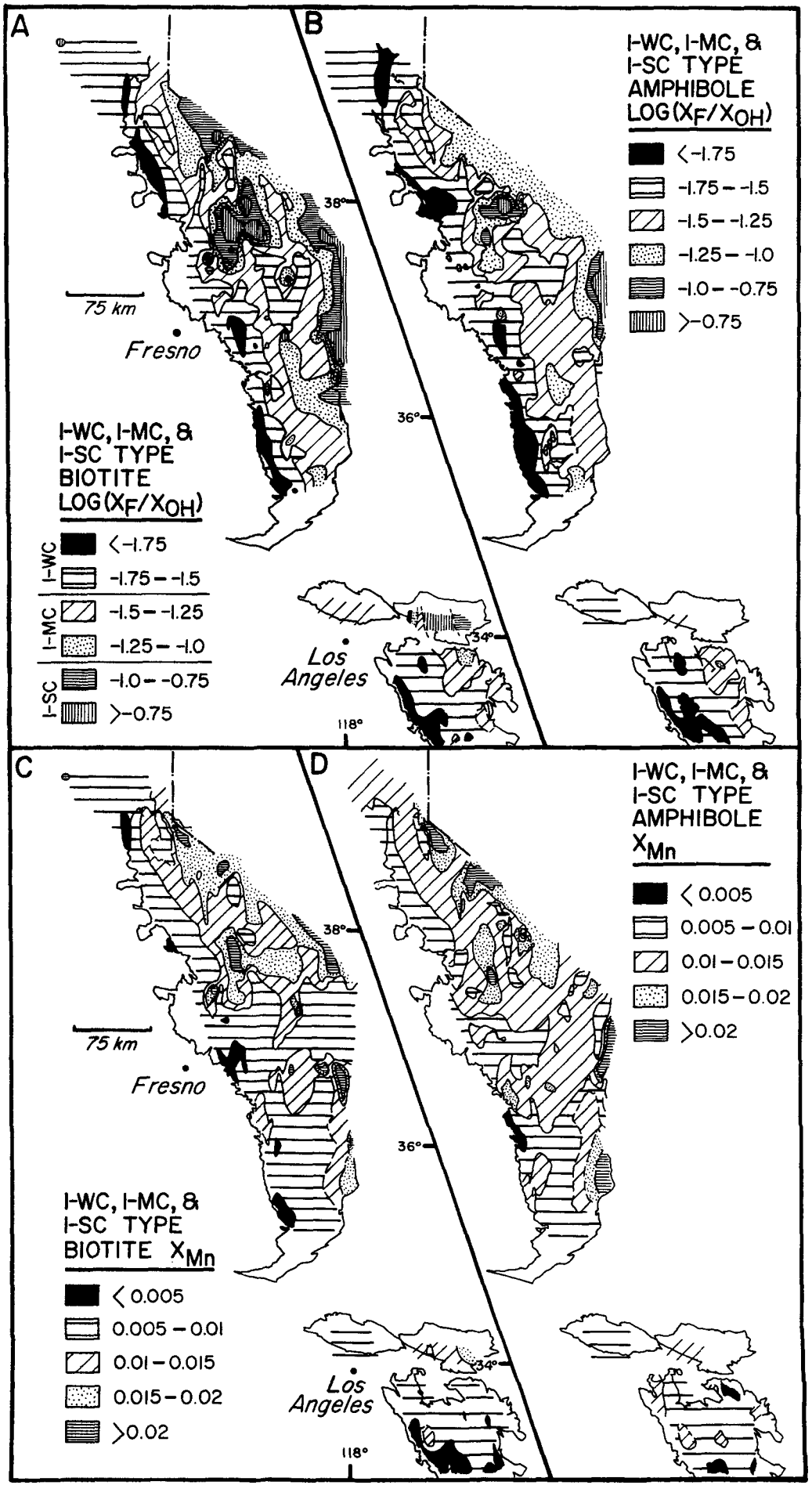

Figure 16. Regional trends in $\log(X_F/X_{OH})$ and X_{Mn} for I-WC-, I-MC-, and I-SC-type biotites and amphiboles (I-SCR types are excluded). A, B. Log (X_F/X_{OH}) contours for biotites and amphiboles. C, D. X_{Mn} contours for biotites and amphiboles. $\log(X_F/X_{OH})$ and X_{Mn} both increase systematically from west to east across the batholiths, although regions of $\log(X_F/X_{OH}) < -1.5$ may occur in the eastern SNB.

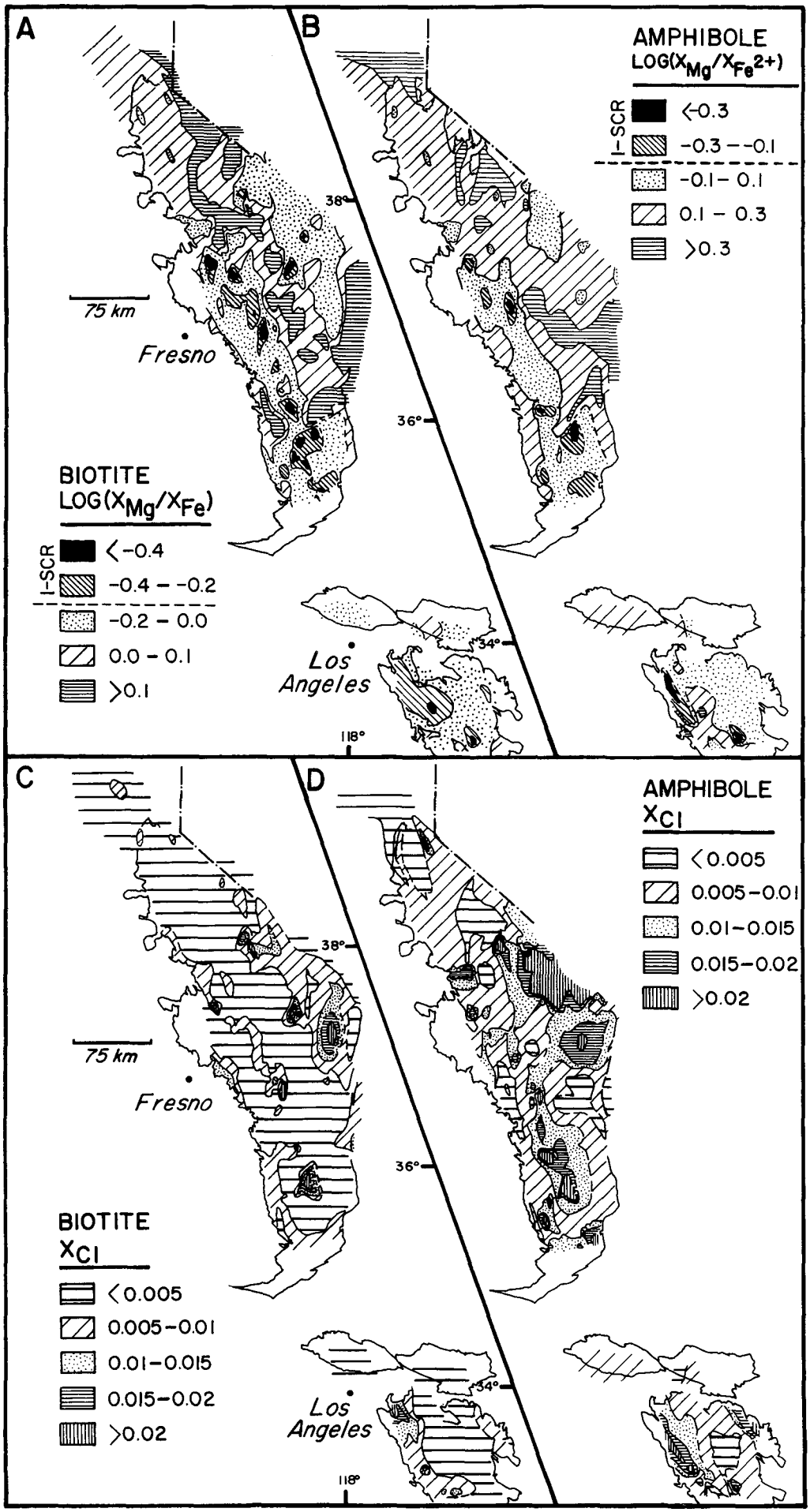

Figure 17. Regional systematics of $\log(X_{Mg}/X_{Fe})$ and X_{Cl} in biotites and amphiboles of I-WC, I-MC, I-SC, and I-SCR types. A, B. $\text{Log}(X_{Mg}/X_{Fe})$ contours for biotites and amphiboles. All Fe is taken as FeO for biotites, but calculated values of Fe^{2+} are used for amphiboles. Regions of Mg-poor silicates (biotite $\log(X_{Mg}/X_{Fe}) < -0.2$; amphibole $\log(X_{Mg}/X_{Fe^{2+}}) < -0.1$) correspond to I-SCR granites. C, D. X_{Cl} in biotites and amphiboles. Regions of high X_{Cl} correspond to occurrence of Fe-rich I-SCR silicates and are also found in the eastern SNB and PRB associated with more Mg-rich mafic phases.

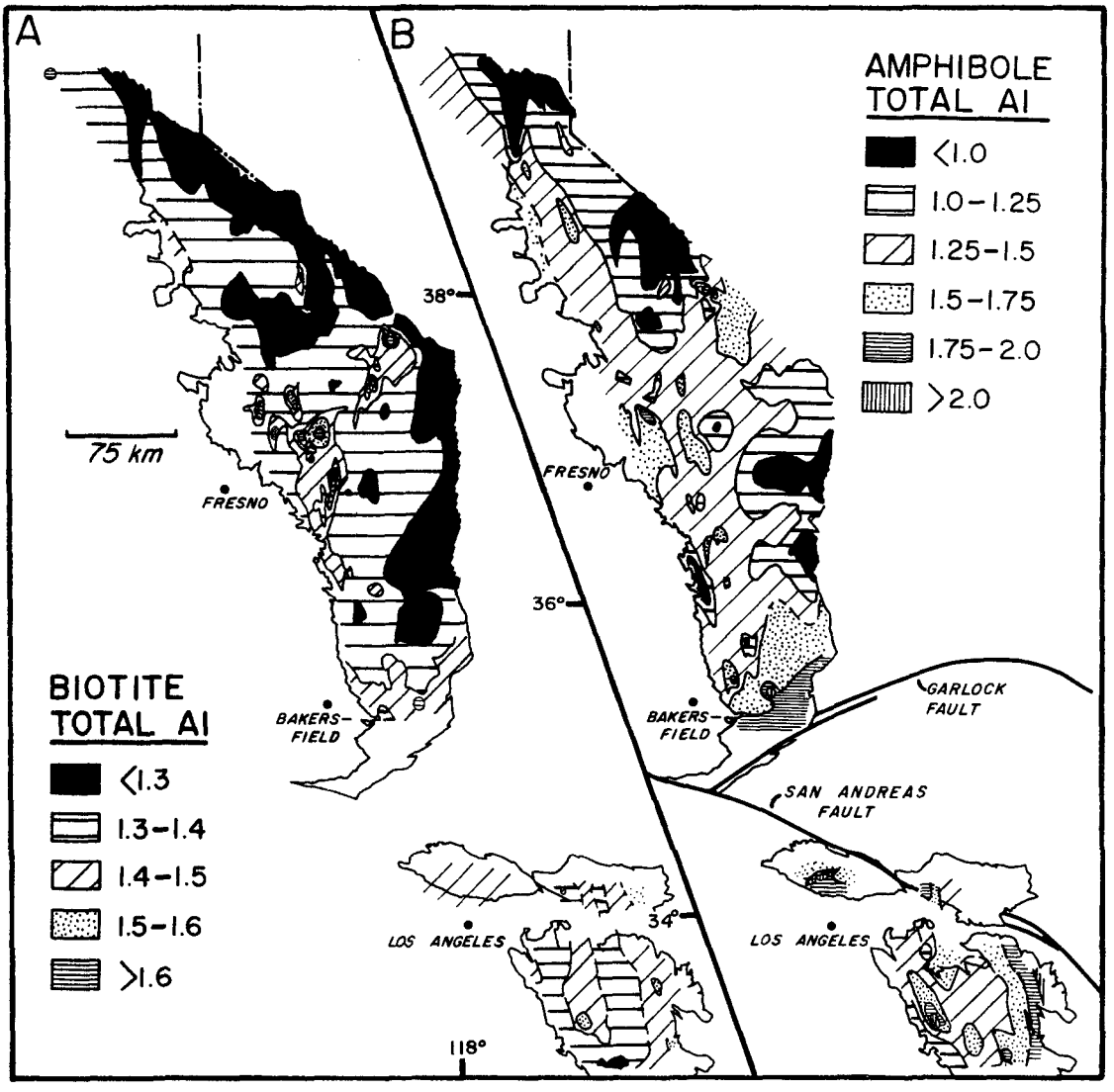

Figure 18. Regional contours of total aluminum (formula units) in biotites and amphiboles of I-WC, I-MC, I-SC, and I-SCR types. A. Regions of high total Al (>1.5) generally occur where biotite coexists with aluminous phases such as muscovite, garnet, and tourmaline (compare with Fig. 14). B. Al in amphibole. Note broad west-to-east decreases in Al in SNB and west-to-east increases in the Al in PRB. The SGB shows highest overall amphibole Al content.

the highest F content attained is that of the I-MC types of the San Jacintos. The rocks of the SGB are generally of I-MC type, but we note that the occurrence of I-SC types is restricted to the western part of the range. Differences in the biotite and amphibole regional systematics are largely due to the fact that many I-SC and I-SCR samples contain biotite but no amphibole. The contours of amphibole compositional parameters thus are derived from fewer data than are the ones for biotite.

As is the case with F/OH, Mn increases from west to east across the batholiths, owing to the incompatible behavior of Mn in silicate magmas. The highest Mn values are found in the eastern SNB and SBB, associated with I-SC granites (Figs. 16C, 16D). We have omitted the I-SCR types from the contoured data set for clarity.

The regional variations in $\log(X_{Mg}/X_{Fe})$ highlight the presence of I-SCR types (Figs. 17A, 17B). Here, all granitic rock types (I-WC, I-MC, I-SC, and I-SCR) have been contoured as one data set. Except for isolated plutons in the eastern SNB and PRB, the Fe-rich silicates [$\log(X_{Mg}/X_{Fe}) < -0.2$ for biotite; $\log(X_{Mg}/X_{Fe^{2+}}) < -0.1$ for amphiboles] are restricted to narrow northwest-trending belts in the western SNB and PRB corresponding to the occurrence of I-SCR granites. In contrast, the highest values of $\log(X_{Mg}/X_{Fe})$ are generally found in the northern and eastern SNB samples.

Figures 17C and 17D show regional variations in X_{Cl}. All I-WC, I-MC, I-SC, and I-SCR types have been contoured as a group in this plot. Although the patterns are not exceedingly well defined, the highest values are associated with the Fe-rich silicates of I-SCR affinity and, somewhat surprisingly, some of the Mg-rich silicates of the eastern SNB and PRB. "Mg-Cl avoidance" (Munoz, 1984) is not the sole controlling factor in regional variation of Cl content. Inspection of Figures 17C and 17D demonstrates that amphiboles typically have higher X_{Cl} than do coexisting biotites (see Fig. 12D).

The regional distributions of total Al in biotite and amphibole are crudely similar but are significantly different in detail. The regions of highest total aluminum in biotite are generally found in association with I-SCR types where biotite coexists with the aluminous phases muscovite, garnet, or tourmaline (Fig. 18A). The lowest Al contents are found in the I-WC–, I-MC–, and I-SC–type biotites of the northern and eastern SNB. In contrast, regional patterns in total Al in amphibole (Fig. 18B) reflect depth of emplacement of the magmas, as deduced elsewhere (Hammarstrom and Zen, 1986). Given the appropriate mineral buffer assemblages, increases in total Al are positively correlated with increases in crystallization pressure (Hammarstrom and Zen, 1986). We note, however, that in Figure 18B, we have included data from all of

the amphibole-bearing samples which we have collected, some of which are mineralogically incompatible with the Hammarstrom and Zen (1986) barometer. In detail, therefore, some aspects of the regional distribution of total Al may reflect factors such as magma bulk composition rather than crystallization pressure. The SNB is characterized by broad west-to-east decreases in total Al in amphibole (Fig. 18B). In addition, an extensive region of high total Al (greater than 1.75 f.u.) is present in the southern SNB near the Garlock fault. The PRB shows a general west-to-east increase in total aluminum in amphibole with regions of highest Al content being situated to the east of the eastern Peninsular Ranges mylonite zone (Fig. 1; Erskine, 1985). The SGB shows the highest over-all aluminum in amphibole, with an average value of about 1.9 f.u. Depths of emplacement are discussed in detail in Ague and Brimhall (1988).

Pre-batholithic Roof Pendant Terranes

Through magmatic processes such as assimilation and partial melting, geochemically distinct pre-batholithic wall-rock terranes may strongly modify the chemistry and petrologic character of magmas which intrude them (compare with Farmer and DePaolo, 1983; Ague and Brimhall, 1987). Although the roof pendants of the batholiths comprise a diverse spectrum of rock types which range in age from Precambrian to Cretaceous, we focus our attention upon the pre-batholithic terranes containing chemically reactive reduced pelitic sedimentary material because of the close spatial association of these terranes with I-SCR intrusives.

In the main portion of the SNB, roof pendants containing graphite-bearing pelitic material are restricted primarily to the Late Triassic to Early Jurassic Kings terrane (Nokleberg, 1983) (Fig. 19). Isolated pelitic rocks also occur in pendants farther east within the Carboniferous to Permian age High Sierra terrane and the Cambrian to Silurian (?) age Owens terrane (Nokleberg, 1983). Similar rocks of Triassic to Jurassic age are present to the south in the PRB and comprise the Bedford Canyon Formation of Larsen (1948), the French Valley Formation of the Hemet area, and the Julian schist of San Diego County (Gastil, 1985).

The Kings terrane consists predominantly of quartzites and schists, with lesser amounts of marble, metadacite tuff, ash-flow tuff, and volcanic breccia (Saleeby and others, 1978; Nokleberg, 1983). The clastic formations of the PRB are similar lithologically. The first comprehensive characterization of these rocks is Larsen's (1948) work on the Bedford Canyon Formation, which he described as being made up of slates, argillites, minor quartzite, and rare lenses of limestone. Mineralogically, the pelites typically contain quartz, muscovite, and biotite with lesser plagioclase, orthoclase, garnet, cordierite, and aluminosilicates and accessory magnetite, perthitic feldspar, tourmaline, rutile, zircon, and sphene (Larsen, 1948; Schwarcz, 1969). In addition, carbonaceous material is an important constituent of the pelitic wall rocks (Knopf and Thelen, 1905; Durrell, 1943; Larsen, 1948; Dibblee and Chesterman, 1953; Plafker, 1956; Bateman, 1965; Schwarcz, 1969; Saleeby and others, 1978). For example, Schwarcz (1969), in his study of the rocks of the Winchester area in the northern PRB found that pelitic schists may contain as much as 15 modal % graphite. The rocks of the pendants range in metamorphic grade from biotite grade or less to garnet-sillimanite migmatitic gneisses (Larsen, 1948; Schwarcz, 1969). We note that in the southern part of the I-SCR belt in the SNB, granitic rocks contain numerous high-grade metamorphic quartz-mica schist xenoliths (Dibblee and Chesterman, 1953).

Saleeby and others (1978) interpreted the Kings terrane of the SNB to represent a submarine fan system containing cratonally derived sand and volcanic material intercalated with shales, marls, and carbonates. Deposition of the PRB wall rocks is ascribed to proximal or more distal turbidity currents in a submarine fan environment (Gastil, 1985; Todd and others, 1988). What is crucial regarding the marine depositional environments of these sequences is that locally, conditions were reducing enough so that organic matter was deposited and preserved within the fine-grained sediments.

Graphite-bearing pelitic wall rocks apparently do not comprise a significant portion of either the San Gabriels or the SBB. The wall rocks of the San Gabriel block are Precambrian metamorphic and igneous rocks along with exotic metasediments of oceanic affinity emplaced, probably by subduction processes, after the main phase of Mesozoic plutonism (Ehlig, 1981). SBB pendants also contain Precambrian rocks and, in addition, lower Paleozoic marbles and quartzites.

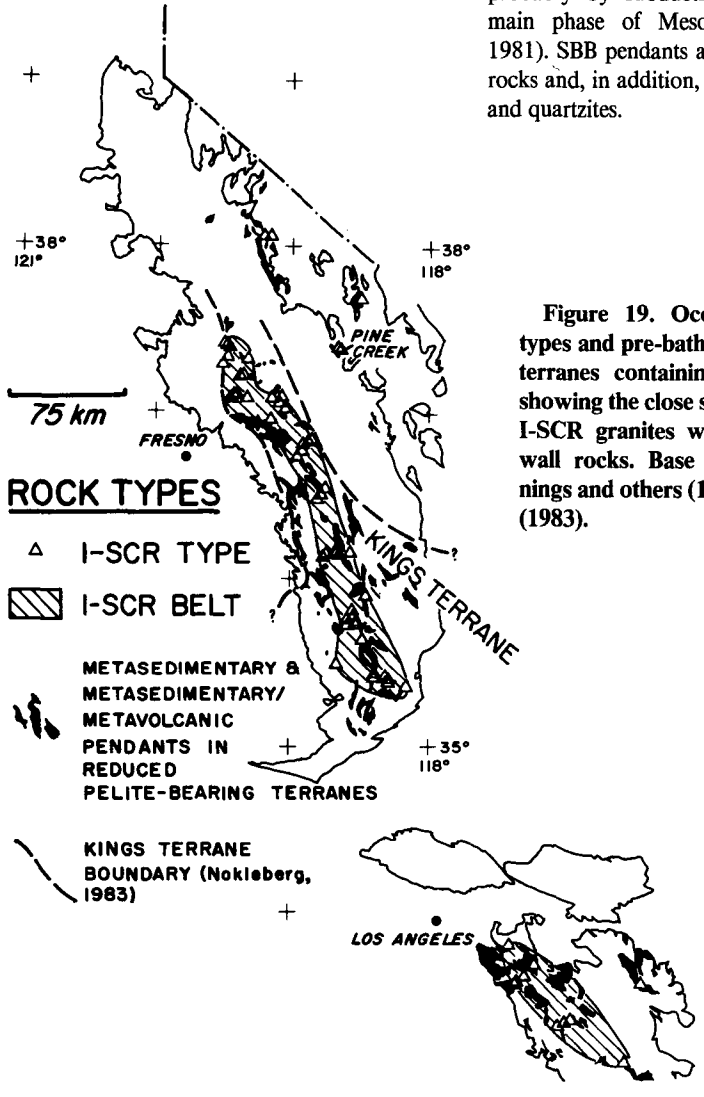

Figure 19. Occurrence of I-SCR types and pre-batholithic roof-pendant terranes containing graphitic pelites, showing the close spatial association of I-SCR granites with highly reducing wall rocks. Base geology from Jennings and others (1977) and Nokleberg (1983).

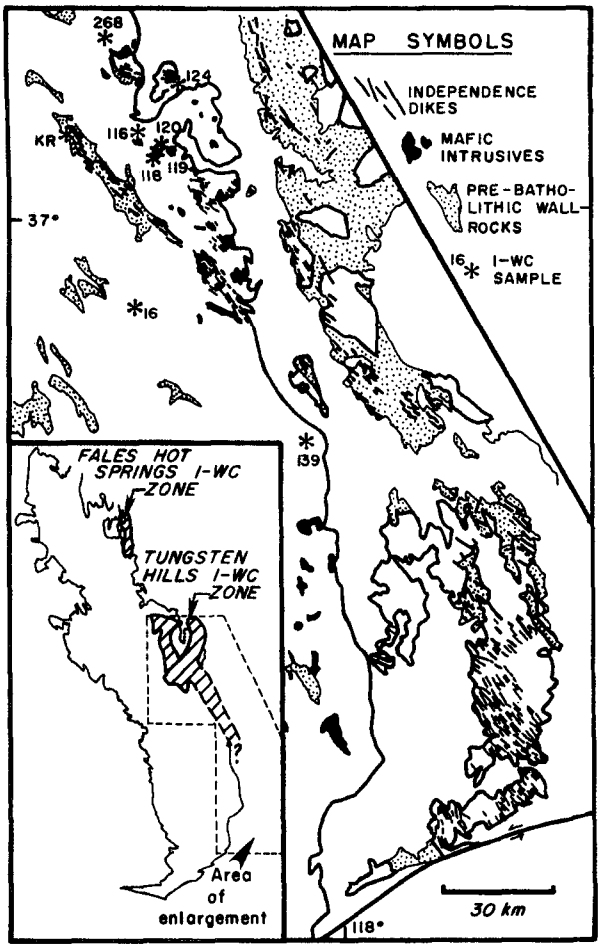

Figure 20. Distribution of I-WC types in eastern Sierra Nevada batholith. Insert shows Fales Hot Springs and Tungsten Hills I-WC zones. Enlargement illustrates spatial association of I-WC types of Tungsten Hills I-WC zone with mafic intrusives and Independence dike swarm of eastern SNB. Base geology from Jennings and others (1977) and Chen and Moore (1979).

Figure 19 illustrates the occurrence of I-SCR plutons in relation to the pendant terranes containing reduced pelitic rocks. It is immediately obvious that a remarkable correlation exists between the locations of the pelitic sedimentary wall-rock terranes and the I-SCR plutons. Equally impressive is the lack of I-SCR plutons and graphite-bearing roof pendants north of approximately latitude 37°30′N. in the SNB and within the regions we have sampled in the SBB and SGB. The close spatial association of I-SCR intrusives with terranes containing reduced pelitic wall rocks strongly suggests that they are genetically related.

I-WC Types of the Eastern Sierra Nevada Batholith

As discussed above, I-WC intrusives may occur in both the western and eastern Sierra Nevada batholith. The presence of I-WC quartz diorites and granodiorites in the eastern Sierra, however, is at variance with the general west-to-east petrologic trend toward more silicic plutons in the eastern portions of the batholith. There is a small region of I-WC magmatism in the northeastern Sierra Nevada batholith and a more extensive I-WC zone in the central-eastern part of the range. These eastern regions where I-WC types may occur are herein referred to as the "Fales Hot Springs" and "Tungsten Hills" I-WC zones (Fig. 20).

Several important geologic and petrologic features correlate with the zones of anomalous I-WC magmatism. First, mafic intrusive rocks occur as isolated bodies along the eastern margin of the batholith in the vicinity of both the Fales Hot Springs and Tungsten Hills I-WC zones (compare with Bateman, 1965; Kistler and Peterman, 1973). In the Tungsten Hills region, the mafic intrusives range in age from Triassic to Late Cretaceous (Fig. 20) (Bateman, 1965; Stern and others, 1981; Frost, 1986). Second, the position of the Tungsten Hills I-WC zone correlates with the northern portion of the Upper Jurassic Independence dike swarm (Moore and Hopson, 1961), a geologic feature which is most probably a manifestation of crustal thinning (Fig. 20) (Chen and Moore, 1979). As discussed in detail in Ague and Brimhall (1988), the spatial association of eastern I-WC types with mafic intrusives and the Independence dike swarm suggests that I-WC magmas intruded a region of anomalously thin or perhaps absent continental crust in the eastern Sierra which may have persisted throughout the Mesozoic.

DISCUSSION AND CONCLUSIONS

We have demonstrated that spatial variations in whole-rock geochemistry and mafic and accessory mineral compositions define both smooth regional-scale gradients and abrupt local-scale discontinuities in the batholiths of California. In the presence of appropriate mineral buffer assemblages, the variations in mineral chemistry indicate differences in critical magmatic intensive variables which in turn provide important constraints upon the geochemical character of the magmatic source components involved in pluton formation and the petrologic evolution of the batholiths. The reasons for these variations and their importance in elucidating processes of batholith development are detailed in Ague and Brimhall (1988), but we summarize the general implications of the regional variations in geochemistry here.

Both $\log(X_F/X_{OH})$ and X_{Mn} in mafic silicates display regional-scale west-to-east increases from I-WC to I-MC and I-SC types, broadly reflecting the incompatible nature of F and Mn. At a more fundamental level, the variation in $\log(X_F/X_{OH})$ illustrates eastward increases in f_{HF}/f_{H_2O} attending magma crystallization and indicates that at least one of the source components of the eastern magmas was more enriched in F relative to H_2O than the source(s) of the western plutons. The regional gradients in whole-rock geochemistry and mineral chemistry imply the involvement of highly differentiated materials with elevated F/H_2O, most probably derived from the continental craton of western North America, in the formation of the eastern I-MC and I-SC intrusives. I-WC quartz diorites and granodiorites also occur in the eastern Sierra Nevada batholith, associated primarily with regions of crustal thinning active at least as far back as Jurassic time. In addition, although high values of X_{Cl} are generally found in the Fe-rich I-SCR silicates owing to the low energy of the Fe-Cl bond in the structure of mafic phases (Mg-Cl avoidance; Munoz, 1984), significant regions of Mg- and Cl-rich ferromagnesian phases occur in the eastern SNB and PRB, which implies the involvement of a Cl-rich source in the generation of these magmas.

In contrast to the regional-scale compositional variations defined by the I-WC, I-MC, and I-SC intrusives, the I-SCR granites generally

occur in north-northwest–striking belts which locally disrupt regional west-to-east gradients in mineral composition and whole-rock geochemistry. Given the granite buffer assemblage (Wones and Eugster, 1965), the Fe-rich biotites of I-SCR granites indicate low oxygen fugacities of crystallization when compared to the other rock types. The distinctive geochemical character and low oxygen fugacities of crystallization of the I-SCR granites, coupled with their occurrence within pre-batholithic wall-rock terranes containing highly reducing pelites, strongly suggest that graphitic pelites are an essential source component or assimilant of the I-SCR intrusives.

Regions of high total Al in biotite (>1.5 f.u.) generally correlate with the occurrence of strongly peraluminous I-SCR types where the activity of siderophyllite is fixed at a high level by coexisting aluminous minerals such as muscovite and garnet. Total Al in amphibole displays regional-scale variations which unlike F/OH, do not reflect variations in magmatic source materials but instead indicate the depth of crystallization of the plutons (Hammarstrom and Zen, 1986).

In summary, the regional variations in mineral chemistry which we have elucidated in the California batholiths are strong functions of magmatic intensive variables. In Ague and Brimhall (1988), we quantify f_{HF}/f_{H_2O}, f_{HF}/f_{HCl}, T-f_{O_2} relations and crystallization pressures and couple this information with whole-rock geochemical systematics of the intrusive types and published isotopic and age data in order to contribute further to our understanding of magma generation in calc-alkaline volcano-plutonic arcs.

ACKNOWLEDGMENTS

We are indebted to I.S.E. Carmichael, C. N. Alpers, D. M. Walniuk, and Chris Lewis for many insightful discussions which have contributed substantially to this study. We thank R. W. Kistler for his thoughtful review of this paper. John Donovan maintained the electron microprobe and provided technical innovations which facilitated the accurate analysis of light elements. Joachim Hampel carefully performed the whole-rock XRF analyses. Tim Teague prepared numerous polished thin sections and probe mounts. Sharie Shute assisted in the compilation of pluton names.

APPENDIX 1. WHOLE-ROCK ANALYSES

Sample*	I-WC					I-MC					I-SC					I-SCR				
	1	3	24	68	69	11	14	62	64	65	17	56	58	59	60	8	9	12	30	34
SiO_2	58.2	59.6	67.6	62.9	54.1	64.5	64.0	71.5	67.6	72.2	77.3	70.6	71.5	72.4	72.6	73.6	73.3	76.6	73.7	69.4
TiO_2	0.74	0.68	0.51	0.67	0.88	0.94	0.90	0.44	0.67	0.45	0.21	0.55	0.39	0.54	0.52	0.35	0.29	0.32	0.35	0.57
Al_2O_3	17.1	17.2	16.1	16.0	16.2	15.4	15.7	15.0	15.4	14.7	12.5	14.5	15.3	14.4	14.4	14.6	14.9	12.9	13.5	14.6
FeO	6.51	5.87	3.97	5.74	7.93	5.22	4.65	2.04	3.31	1.99	0.39	2.24	1.25	2.45	2.45	1.96	1.29	1.26	1.80	3.00
MgO	3.79	3.07	1.72	2.95	5.52	2.47	2.13	0.73	1.51	0.92	0.22	0.52	0.32	0.87	0.86	0.30	0.31	0.29	0.45	1.11
MnO	0.12	0.11	0.09	0.11	0.14	0.10	0.08	0.05	0.06	0.05	0.04	0.06	0.05	0.07	0.07	0.05	0.04	0.04	0.04	0.06
CaO	7.01	6.48	4.38	5.90	7.78	4.36	4.49	2.89	3.77	2.68	0.62	1.86	1.94	2.83	2.76	1.49	1.36	1.24	2.05	3.26
Na_2O	2.83	3.58	3.88	2.96	2.66	3.30	3.52	3.67	3.99	4.02	3.50	3.77	3.89	4.07	4.33	3.93	3.45	3.13	4.08	3.66
K_2O	1.40	1.17	1.95	2.33	2.43	2.71	3.17	3.74	3.23	3.49	4.77	4.84	4.43	2.77	2.79	3.98	4.16	3.97	2.96	3.10
P_2O_5	0.10	0.13	0.05	0.13	0.26	0.16	0.22	0.11	0.13	0.07	0.02	0.07	0.07	0.15	0.14	n.d.	n.d.	n.d.	n.d.	0.08
Total	97.80	97.89	100.25	99.69	97.90	99.16	98.86	100.17	99.67	100.57	99.57	99.01	99.14	100.55	100.92	100.26	99.10	99.75	98.93	98.84
Ni	19	395	n.d.†	n.d.	52	n.d.	14	n.d.	n.d.	n.d.	n.d.	11	n.d	n.d.	n.d.	n.d	n.d	n.d	n.d	n.d
Cr	39	40	27	42	87	49	15	14	31	18	44	9	10	39	17	56	58	41	24	14
Cu	71	49	17	19	320	7	26	11	11	8	5	14	8	10	8	10	12	9	10	4
Zn	70	73	72	66	78	68	54	31	59	41	7	32	38	62	49	52	39	23	37	43
Rb	47	34	65	78	91	105	104	116	110	107	233	215	169	143	137	179	142	173	95	113
Sr	291	333	334	362	539	406	621	453	543	409	68	263	562	554	552	164	220	176	161	349
Ba	348	454	662	1065	747	689	1238	781	941	854	304	1077	1209	530	530	972	964	670	931	968
Ga	18	16	18	21	19	19	19	20	20	18	18	19	20	19	22	22	18	17	16	17
Zr	125	107	118	151	100	177	178	127	146	125	122	241	126	148	146	180	124	136	142	184
Nb	8	7	11	12	10	17	16	11	11	9	31	16	10	13	16	14	14	17	8	14

*All samples listed in this and the following appendix belong to sample set 1011.
†Not detected.

APPENDIX 2. MODAL ANALYSES

Sample	I-WC					I-MC					I-SC					I-SCR				
	1	24	49	311	376	11	14	62	97	123	17	60	137	152	362	12	34	314	418	423
Alkali feldspar	1.0	14.4	3.9	4.2	6.0	12.4	9.8	20.9	31.5	27.0	30.4	22.4	49.9	26.1	45.9	30.5	27.4	24.3	33.8	39.8
Quartz	16.6	29.9	18.6	6.0	11.2	24.8	18.2	22.3	17.8	18.8	48.8	28.4	26.8	37.4	11.4	41.3	36.3	31.2	24.4	29.7
Plagioclase	59.1	35.0	38.3	61.7	65.2	36.0	32.8	46.7	28.1	41.5	17.6	43.7	20.0	25.8	36.0	22.1	22.9	28.8	29.9	20.2
Biotite	7.4	7.1	10.7	14.5	7.7	18.7	29.2	4.4	17.7	6.0	1.7	2.5	1.8	7.3	4.6	5.0	9.4	4.0	1.3	1.1
Amphibole	11.1	10.2	24.5	8.1	8.1	5.3	5.5	4.2	2.4	5.4	··	1.2	··	··	··	··	3.8	··	··	··
Orthopyroxene	0.8	··	··	··	··	··	··	··	··	··	··	··	··	··	··	··	··	··	··	··
Clinopyroxene	3.5	··	··	··	··	··	··	··	··	··	··	··	··	··	··	··	··	··	··	··
Muscovite	··	··	··	··	··	··	··	··	··	··	··	··	··	··	··	0.5	··	7.8	8.3	6.5
Garnet	··	··	··	··	··	··	··	··	··	··	··	··	··	··	··	··	··	··	1.8	2.6
Chlorite	··	0.28	0.51	··	··	0.13	··	0.26	··	0.16	tr	··	··	1.6	1.2	tr	tr	3.8	0.41	tr
Epidote	··	0.82	2.7	0.37	tr	0.15	tr	··	0.26	0.15	··	··	··	··	··	tr	··	··	··	··
Magnetite	0.36	1.2	··	3.4	1.1	0.95	1.5	0.63	1.3	0.86	0.43	0.66	1.23	1.0	0.24	0.12	··	··	··	··
Ilmenite	0.12	0.39	0.69	0.30	0.60	··	··	··	··	··	0.43	··	0.2	··	··	0.5	tr	0.10	0.14	0.10
Sphene	··	··	··	1.3	··	1.5	2.9	0.34	0.19	0.20	0.11	0.89	··	0.55	0.69	··	··	··	··	··
Sericite	··	tr	0.1	··	··	··	··	··	··	··	0.33	tr	··	tr	··	··	tr	··	··	··
Apatite	tr*	0.59	tr	tr	tr	tr	tr	tr	tr	tr	tr	0.11	tr	0.11	0.10	tr	tr	tr	tr	tr

*tr < 0.1

REFERENCES CITED

Ague, J. J., and Brimhall, G. H., 1987, Granites of the batholiths of California: Products of local assimilation and regional scale contamination: Geology, v. 15, p. 63–66.

——1988, Magmatic arc asymmetry and distribution of anomalous plutonic belts in the batholiths of California: Effects of assimilation, crustal thickness, and depth of crystallization: Geological Society of America Bulletin, v. 100, p. 912–927 (this issue).

Akima, H., 1978, A method of bivariate interpolation and smooth surface fitting for irregularly distributed data points: Association for Computing Machinery Transactions on Mathematical Software, v. 4, p. 148–159.

Albee, A. L., and Ray, L., 1970, Correction factors for electron probe microanalysis of silicates, oxides, carbonates, phosphates, and sulfates: Analytical Chemistry, v. 42, p. 1408–1414.

Albers, J. P., 1981, A lithologic-tectonic framework for the metallogenic provinces of California: Economic Geology, v. 76, p. 765–790.

Anderson, A. T., 1980, Mineral equilibria and crystallization conditions in the late Precambrian Wolf River massif, Wisconsin: American Journal of Science, v. 280, p. 298–332.

Bateman, P. C., 1965, Geology and tungsten mineralization of the Bishop district, California: U.S. Geological Survey Professional Paper 470, 208 p.

Bateman, P. C., and Chappell, B. W., 1979, Crystallization, fractionation, and solidification of the Tuolumne intrusive series, Yosemite National Park, California: Geological Society of America Bulletin, v. 90, p. 465–482.

Bateman, P. C., and Dodge, F.C.W., 1970, Variations in major chemical constituents across the central Sierra Nevada batholith: Geological Society of America Bulletin, v. 81, p. 409–420.

Bateman, P. C., Kistler, R. W., Peck, D. L., and Busacca, A., 1983, Geologic map of the Tuolumne Meadows quadrangle, Yosemite National Park, California: U.S. Geological Survey Quadrangle Map GQ-1570.

Bence, A. E., and Albee, A. L., 1968, Empirical correction factors for the electron probe microanalysis of silicates and oxides: Journal of Geology, v. 76, p. 382–403.

Brady, J. B., 1974, Coexisting actinolite and hornblende from west central New Hampshire: American Mineralogist, v. 59, p. 529–535.

Brimhall, G. H., 1979, Lithologic determination of mass transfer mechanisms of multiple-stage porphyry copper mineralization at Butte, Montana: Vein formation by hypogene leaching and enrichment of potassium silicate protore: Economic Geology, v. 74, p. 556–589.

Brimhall, G. H., and Ague, J. J., 1988, Granitic systems, *in* Barnes, H. L., and Ohmoto, H., eds., Hydrothermal processes—Applications to ore genesis: Dordrecht, Holland, Reidel (in press).

Brimhall, G. H., and Rivers, M. L., 1985, Semi-automatic optical scanning apparatus utilizing line integration: U.S. patent number 4,503,555, 21 p.

Brimhall, G. H., Gilzean, M., and Burnham, C. W., 1983, Magmatic source region, protoliths and controls on metallogenesis: Mica halogen chemistry [abs.]: EOS (American Geophysical Union Transactions), v. 64, p. 884.

Brimhall, G. H., Agee, C., and Stoffregen, R., 1985, The hydrothermal conversion of hornblende to biotite: Canadian Mineralogist, v. 23, p. 369–379.

Carmichael, I.S.E., 1967, The iron-titanium oxides of salic volcanic rocks and their associated ferromagnesian silicates: Contributions to Mineralogy and Petrology, v. 14, p. 36–64.

Chappell, B. W., and White, A.J.R., 1974, Two contrasting granite types: Pacific Geology, v. 8, p. 173–174.

Chen, J. H., and Moore, J. G., 1979, The Late Jurassic Independence dike swarm in eastern California: Geology, v. 7, p. 129–133.

——1982, Uranium-lead isotopic ages from the Sierra Nevada batholith, California: Journal of Geophysical Research, v. 87, p. 4761–4784.

Collins, W. J., Beams, S. D., White, A.J.R., and Chappell, B. W., 1982, Nature and origin of A-type granites with particular reference to southeastern Australia: Contributions to Mineralogy and Petrology, v. 80, p. 189–200.

Czamanske, G. K., Ishihara, S., and Atkin, S. A., 1981, Chemistry of rock-forming minerals of the Cretaceous-Paleocene batholith in southwestern Japan and implications for magma genesis: Journal of Geophysical Research, v. 86, p. 10431–10469.

Deer, W. A., Howie, R. A., and Zussman, J., 1966, An introduction to the rock-forming minerals: London, United Kingdom, Longman, 528 p.

DePaolo, D. J., 1981, A neodymium and strontium isotopic study of the Mesozoic calc-alkaline granitic batholiths of the Sierra Nevada and Peninsular Ranges, California: Journal of Geophysical Research, v. 86, p. 10470–10488.

Dibblee, T. W., Jr., and Chesterman, C. W., 1953, Geology of the Breckenridge Mountain quadrangle, California: California Division of Mines Bulletin 168, 56 p.

Dickinson, W. R., 1970, Relations of andesites, granites and derivative sandstones to arc-trench tectonics: Reviews of Geophysics and Space Physics, v. 8, p. 813–860.

Dodge, F.C.W., 1972, Variation of ferrous-ferric ratios in the central Sierra Nevada batholith, U.S.A.: International Geological Congress, 24th, section 10, Montreal, p. 12–19.

Dodge, F.C.W., Moore, J. G., Papike, J. J., and Mays, R. E., 1968, Hornblendes from granitic rocks of the central Sierra Nevada batholith, California: Journal of Petrology, v. 9, p. 378–410.

Dodge, F.C.W., Smith, V. C., and Mays, R. E., 1969, Biotites from the granitic rocks of the central Sierra Nevada batholith, California: Journal of Petrology, v. 10, p. 250–271.

Durrell, C., 1943, Geology of the Sierra Nevada northeast of Visalia, Tulare County, California: California Journal of Mines and Geology, v. 39, p. 153–168.

Early, T. O., and Silver, L. T., 1973, Rb-Sr isotopic systematics in the Peninsular Ranges batholith of southern and Baja California [abs.]: EOS (American Geophysical Union Transactions), v. 54, p. 494.

Ehlig, P. L., 1981, Origin and tectonic history of the basement terrane of the San Gabriel Mountains, central Transverse Ranges, *in* Ernst, W. G., ed., The geotectonic development of California: Englewood Cliffs, New Jersey, Prentice-Hall, p. 253–283.

Erskine, B. G., 1985, Mylonitic deformation and associated low-angle faulting in the Santa Rosa mylonite zone, southern California [Ph.D. thesis]: Berkeley, California, University of California, 247 p.

Evernden, J. F., and Kistler, R. W., 1970, Chronology of emplacement of Mesozoic batholithic complexes in California and western Nevada: U.S. Geological Survey Professional Paper 623, 42 p.

Farmer, G. L., and DePaolo, D. J., 1983, Origin of Mesozoic and Tertiary granite in the western United States and implications for pre-Mesozoic crustal structure 1. Nd and Sr isotopic studies in the geocline of the northern Great Basin: Journal of Geophysical Research, v. 88, p. 3379–3401.

Frost, T. P., 1986, Lamarck granodiorite: Interaction of multiple mafic magmas with felsic magma, Sierra Nevada, California [abs.]: EOS (American Geophysical Union Transactions), v. 67, p. 1268.

Gastil, G., 1985, Terranes of Peninsular California and adjacent Sonora, *in* Howell, D. G., ed., Tectonostratigraphic terranes: Houston, Texas, Circum-Pacific Council for Energy and Mineral Resources, p. 273–284.

Goldschmidt, V. M., 1954, Geochemistry: Oxford, United Kingdom, Clarendon Press, 730 p.

Gunow, A. J., Ludington, S., and Munoz, J. L., 1980, Fluorine in micas from the Henderson molybdenite deposit, Colorado: Economic Geology, v. 75, p. 1127–1137.

Hammarstrom, J. M., and Zen, E-An, 1986, Aluminum in hornblende: An empirical igneous geobarometer: American Mineralogist, v. 71, p. 1297–1313.

Hildreth, W., 1979, The Bishop Tuff: Evidence for the origin of compositional zonation in silicic magma chambers: Geological Society of America Special Paper 180, p. 43–75.

Hill, R. I., Silver, L. T., and Taylor, H. P., Jr., 1986, Coupled Sr-O isotopic variations as an indicator of source heterogeneity for the northern Peninsular Ranges batholith: Contributions to Mineralogy and Petrology, v. 92, p. 351–361.

Ishihara, S., 1977, The magnetite-series and ilmenite-series granitic rocks: Mining Geology, v. 27, p. 293–305.

Jacobs, D. C., and Parry, W. T., 1979, Geochemistry of biotite in the Santa Rita porphyry copper deposit, New Mexico: Economic Geology, v. 74, p. 860–887.

Jennings, C. W., Strand, R. G., and Rogers, T. H., compilers, 1977, Geologic map of California: State of California Department of Conservation, scale 1:7,500,000, 1 sheet.

Kistler, R. W., 1966, Structure and metamorphism in the Mono Craters quadrangle Sierra Nevada, California: U.S. Geological Survey Bulletin 1221-E, 53 p.

——1973, Geologic map of the Hetch Hetchy quadrangle, Yosemite National Park, California: U.S. Geological Survey Quadrangle Map GQ-1112.

——1974a, Hetch Hetchy reservoir quadrangle, Yosemite National Park, California—Analytic data: U.S. Geological Survey Professional Paper 774-B, 15 p.

——1974b, Phanerozoic batholiths in western North America: A summary of some recent work on variations in time, space, chemistry and isotopic compositions: Earth and Planetary Science Letters Annual Review, v. 2, p. 403–418.

Kistler, R. W., and Peterman, Z. E., 1973, Variations in Sr, Rb, K, Na, and initial $^{87}Sr/^{86}Sr$ in Mesozoic granitic rocks and intruded wall rocks in central California: Geological Society of America Bulletin, v. 84, p. 3489–3512.

Kistler, R. W., Chappell, B. W., Peck, D. L., and Bateman, P. C., 1986, Isotopic variation in the Tuolumne intrusive suite, central Sierra Nevada, California: Contributions to Mineralogy and Petrology, v. 94, p. 205–220.

Knopf, A., and Thelen, P., 1905, Sketch of the geology of Mineral King, California: University of California Publications Bulletin of the Department of Geology, v. 4, p. 227–262.

Larsen, E. S., 1948, Batholith and associated rocks of the Corona, Elsinore, and San Luis Rey quadrangles, southern California: Geological Society of America Memoir 29, 182 p.

Lawson, C. L., 1977, Software for C1 surface interpolation: Jet Propulsion Laboratory Publication 77-30.

Lindgren, W., 1915, The igneous geology of the Cordilleras and its problems, *in* Problems of American geology: New Haven, Connecticut, Yale University Press, Silliman Foundation, p. 234–286.

Masi, U., O'Neil, J. R., and Kistler, R. W., 1981, Stable isotope systematics in Mesozoic granites of central and northern California and southwestern Oregon: Contributions to Mineralogy and Petrology, v. 76, p. 116–126.

Miller, C. F., and Stoddard, E. F., 1981, The role of manganese in the paragenesis of magmatic garnet: An example from the Old Woman–Piute Range, California: Journal of Geology, v. 89, p. 233–246.

Moore, J. G., 1959, The quartz diorite boundary line in the western United States: Journal of Geology, v. 67, p. 197–210.

Moore, J. G., and Hopson, C. A., 1961, The Independence dike swarm in eastern California: American Journal of Science, v. 259, p. 241–259.

Munoz, J. L., 1984, F-OH and Cl-OH exchange in micas with applications to hydrothermal ore deposits, *in* Bailey, S. W., ed., Micas: Reviews in Mineralogy, v. 13, p. 469–494.

Munoz, J. L., and Swenson, A., 1981, Chloride-hydroxyl exchange in biotite and estimation of relative HCl/HF activities in hydrothermal fluids: Economic Geology, v. 76, p. 2212–2221.

Nelson, B. K., and DePaolo, D. J., 1985, Rapid production of continental crust 1.7 to 1.9 b.y. ago: Nd isotopic evidence from basement of the North American midcontinent: Geological Society of America Bulletin, v. 96, p. 746–754.

Nokleberg, W. J., 1981, Stratigraphy and structure of the Strawberry Mine roof pendant, central Sierra Nevada, California: U.S. Geological Survey Professional Paper 1154, 18 p.

——1983, Wallrocks of the central Sierra Nevada batholith, California: A collage of accreted tectono-stratigraphic terranes: U.S. Geological Survey Professional Paper 1255, 28 p.

Noyes, H. J., Wones, D. R., and Frey, F. A., 1983, A tale of two plutons: Petrographic and mineralogic constraints on the petrogenesis of the Red Lake and Eagle Peak plutons, central Sierra Nevada, California: Journal of Geology, v. 91, p. 353–379.

Plafker, G., 1956, Geology of the southwest part of the Kaweah quadrangle, California [M.S. thesis]: Berkeley, California, University of California, 45 p.

Reid, J. B., Jr., Evans, O. C., and Fates, D. G., 1983, Magma mixing in granitic rocks of the central Sierra Nevada, California: Earth and Planetary Science Letters, v. 66, p. 243–261.

Saleeby, J. B., 1981, Ocean floor accretion and volcanoplutonic arc evolution of the Mesozoic Sierra Nevada, *in* Ernst, W. G., ed., The geotectonic development of California: Englewood Cliffs, New Jersey, Prentice-Hall, p. 132–181.

Saleeby, J. B., Goodin, S. E., Sharp, W. D., and Busby, C. J., 1978, Early Mesozoic paleotectonic-paleogeographic reconstruction of the southern Sierra Nevada region, *in* Howell, D. G., and McDougall, K. A., eds., Mesozoic paleogeography of the western United States: Pacific Coast Paleogeography Symposium, 2nd, p. 311–336.

Sawka, W. N., Banfield, J. F., and Chappell, B. W., 1986, A weathering-related origin of widespread monzonite in S-type granites: Geochimica et Cosmochimica Acta, v. 50, p. 171–175.

Schwarcz, H. P., 1969, Pre-Cretaceous sedimentation and metamorphism in the Winchester area, northern Peninsular Ranges, California: Geological Society of America Special Paper 100, 63 p.

Silver, L. T., Taylor, H. P., Jr., and Chappell, B. W., 1979, Some petrological, geochemical, and geochronological observations of the Peninsular Ranges batholith near the international border of the U.S.A. and Mexico, *in* Abbott, P. L., and Todd, V. R., eds., Mesozoic crystalline rocks: Geological Society of America annual meeting guidebook, p. 83–110.

Stern, T. W., Bateman, P. C., Morgan, B. A., Newell, M. F., and Peck, D. L., 1981, Isotopic U-Pb ages of zircon from the granitoids of the central Sierra Nevada, California: U.S. Geological Survey Professional Paper 1185, 17 p.

Stout, J., 1971, Four coexisting amphiboles from Telemark, Norway: American Mineralogist, v. 56, p. 212–224.

Sylvester, A. G., Miller, C. F., and Nelson, C. A., 1978, Monzonites of the White-Inyo range, California, and their relation to the calc-alkaline Sierra Nevada batholith: Geological Society of America Bulletin, v. 89, p. 1677–1687.

Taylor, H. P., Jr., and Silver, L. T., 1978, Oxygen isotope relationships in plutonic igneous rocks of the Peninsular Ranges batholith, southern and Baja California, *in* Zartman, R. E., ed., Short papers of the 4th International Conference on Geochronology, Cosmochronology, and Isotope Geology: U.S. Geological Survey Open-File Report 78-701, p. 423–426.

Todd, V. R., Erskine, B. G., and Morton, D. M., 1988, Metamorphic and tectonic evolution of the northern Peninsular Ranges batholith, southern California, *in* Ernst, W. G., ed., Metamorphic and crustal evolution of the western U.S. (Rubey Volume 7): Englewood Cliffs, New Jersey, Prentice-Hall (in press).

Whalen, J. B., Currie, K. L., and Chappell, B. W., 1986, A-type granites: Geochemical characteristics and discrimination [abs.]: Geological Association of Canada–Mineralogical Association of Canada annual meeting, v. 11, p. 144.

White, A.J.R., 1979, Sources of granite magmas [abs.]: Geological Society of America Abstracts with Programs, v. 11, p. 539.

White, A.J.R., and Chappell, B. W., 1977, Ultrametamorphism and granitoid genesis: Tectonophysics, v. 43, p. 7–22.

——1983, Granitoid types and their distribution in the Lachlan fold belt, southeastern Australia, *in* Roddick, J. A., ed., Circum-Pacific plutonic terranes: Geological Society of America Memoir 159, p. 21–34.

White, A.J.R., Clemens, J. D., Holloway, J. R., Silver, L. T., Chappell, B. W., and Wall, V. J., 1986, S-type granites and their probable absence in southwestern North America: Geology, v. 14, p. 115–118.

Wones, D. R., and Eugster, H. P., 1965, Stability of biotite: Experiment, theory, and application: American Mineralogist, v. 50, p. 1228–1272.

MANUSCRIPT RECEIVED BY THE SOCIETY JUNE 29, 1987
REVISED MANUSCRIPT RECEIVED NOVEMBER 9, 1987
MANUSCRIPT ACCEPTED DECEMBER 3, 1987

Printed in U.S.A.